THE ATMOSPHERES OF THE B STARS. III. THE COMPOSITION OF TAU SCORPII

L. H. ALLER, G. ELSTE, AND J. JUGAKU
University of Michigan Observatory
Received October 29, 1956

ABSTRACT

New measurements of line intensities in the spectrum of τ Scorpii, based on coudé plates secured at the Mount Wilson and McDonald Observatories, are discussed with the aid of a model atmosphere and Pecker's theory for medium-strong lines. The computational procedures are described in detail, with a view to their application to other stellar atmospheres. The abundances derived differ from those found by Unsöld and by Traving for three reasons: (1) the newer equivalent widths differ systematically from those found with the older McDonald spectrographs; (2) a slightly different model atmosphere is employed; and (3) a precise theory of line formation is utilized. Different ions of the same element yield different curves of growth, whereas lines formed in the same layers tend to have similar curves of growth.

The agreement between theory and observation is improved with the aid of a differential correction to the model atmosphere, but all ions of all elements cannot be equally well represented by the same model atmosphere. The largest uncertainties appear to come from poor f-values. Helium, carbon, nitrogen, oxygen, and silicon are observed in two stages of ionization; other elements are observed in only one stage of ionization.

I. INTRODUCTION

Since the pioneering work of Russell a generation ago, methods for the quantitative chemical analyses of stellar atmospheres have undergone numerous refinements. Eye-estimates of line intensities have been replaced by equivalent widths, and simple calibration-curves have been replaced by increasingly elaborate curves of growth. Unfortunately, of course, with each refinement the necessary numerical calculations have greatly lengthened, so that it is possible to carry out detailed studies for only a limited number of stars.

Among the stars whose compositions and atmospheres have been extensively discussed, perhaps the best known is the B0 V star known as τ Scorpii, which shows sharp lines. Long a favorite object for those who were primarily interested in wave lengths and identifications, its composition was first studied quantitatively by Unsöld (1941*a*, *b*, 1942, 1944) by curve-of-growth methods. He used plates secured with prism spectrographs at the McDonald Observatory. Neven and de Jager (1954) used an empirical model atmosphere log $g = 3.97$ and based their investigation on Mount Wilson coudé plates. Their results differed from those of Unsöld, in that they found lower temperatures and a much lower helium/hydrogen ratio. Traving (1955) used a theoretical model atmosphere (log $g = 4.8$) which represented fairly well the observations of the continuous radiation and of the hydrogen-line profiles as calculated by the usual Holtsmark theory. For the determination of the abundances of the elements, he used a curve of growth computed with the aid of Minnaert's approximation formula for line profiles. The structure of the atmosphere enters only in the abscissa, which involves the effective number of absorbing particles. He obtained results for the excitation temperature and abundances in good agreement with those found earlier by Unsöld and in sharp disaccord with the results by Neven and de Jager.

In our program on the atmospheres of the B stars it has seemed worthwhile to re-examine the problem of the atmosphere of τ Scorpii. The Neven and de Jager model appears to have much too low a temperature to represent the spectrum of τ Scorpii. Traving's model would appear to provide a much better starting approximation. His

assumed log $g = 4.80$ appears to be substantially too high; he recognizes this difficulty and suggests a revised log $g = 4.45$. His model atmosphere gives an Hγ profile that is too wide; the representation of this line with the aid of the Kolb theory suggested a log $g = 4.30$ (Elste, Jugaku, and Aller 1956). Furthermore, the mass-luminosity relationship indicates a log g more nearly in the neighborhood of 4.30 or 4.00.

It appears to be of interest to see what happens if precise curves of growth are computed for the individual ions. Finally, new observational material has been made available to us for this analysis.

In Section II we discuss the model atmosphere adopted for the problem and compare the predicted and observed gradients and Balmer discontinuities. Section III summarizes the portions of Pecker's theory (1950, 1951) on lines of moderate strength needed for our purposes; Section IV discusses the partition function; and Section V gives the detailed applications of the formulae to the lines of specific elements. In Section VI we describe a method of differential correction. Section VII discusses the results of the analysis.

The model atmosphere required to give a best fit to the observations as interpreted with Pecker's theory for medium-strong lines in pure absorption seems to correspond to log $g = 4.30$ and to a higher over-all temperature than Traving's model by about $\Delta\theta = \Delta(5040/T) = -0.01$. The abundances with respect to hydrogen turn out to be smaller than those found by Traving. Neon, however, appears to be more abundant than oxygen in this star. The ratio of hydrogen to helium is particularly difficult to establish, since the lines of both elements are affected by complicated widening mechanisms.

II. CHOICE OF A MODEL ATMOSPHERE

For the application of a more precise theory of line formation it is necessary to have a good model atmosphere. As a starting approximation, the model atmosphere proposed by Traving appeared to be very satisfactory. Because the surface gravity seemed to be too high, we adopted log $g = 4.30$ but assumed that the same temperature distribution would hold for a model with this lower surface gravity. The new model did not differ markedly from that of Traving. Rigorously, it should have been tested for constancy of flux and the necessary adjustments made in the temperature distribution. At the same time an improved composition should have been used, and several other refinements, such as an allowance for the effects of the Lyman lines, should have been introduced. With the present state of our knowledge of f-values and measured line intensities, such improvements would not justify the labor involved. Actually, a network of models for different surface gravities, effective temperatures, and hydrogen/helium ratios should be calculated, giving the following quantities: Balmer discontinuity, absolute gradients, and several sensitive line-intensity ratios. Then it should be possible to find the right models for different stars by comparison with the observed quantities. On the other hand, it is possible that no interpolated or calculated model would fit all the observations. The discrepancies would indicate at what point our theory of line formation in hot stars has to be improved. Such a procedure may become possible eventually, but at the moment the only practical way seems to be to choose the most likely model atmosphere and obtain an improved fit with the observations with the aid of a differential correction.

This revised Traving model, hereafter referred to as "model II," then served as the basis for the prediction of the profile of Hγ and the curves of growth for the lines of Si III and Si IV. It represented these data to within the limits of observational error; hence we employed it for calculations pertaining to other elements.

The comparison between the predicted gradients and Balmer discontinuities and the observed values is given in Table 1. The observed gradients are steeper than the ones predicted by model II. They may be affected by a small amount of space reddening that would tend to produce a steepening which would be more pronounced in the ultraviolet. The failure of both model atmospheres to reproduce the observations must be regarded

as a shortcoming of the theory which will have to be remedied before the models can be regarded as fully adequate.

Table 2 gives certain of the essential parameters of the atmosphere. Column 1 lists $\theta = 5040/T$; column 2 gives $x = \log \tau_{\lambda_0}$; column 3 gives $\log P_e$; and column 4 gives $\log (\kappa_0 + \sigma)$. Here κ_0 and τ_{λ_0} are the continuous absorption coefficients and optical depths at λ 4000 A. Additional quantities that have to be calculated for the model atmosphere will be described in Sections III, IV, and V.

III. THEORY OF THE LINE SPECTRUM

We shall now assemble the necessary equations for an analysis of the equivalent widths of medium-strong lines. Consider a point on a star's surface from which the ray directed to the observer includes an angle ϑ with the outward normal. The line depth at a wave-length difference $\Delta\lambda$ from the center of a line formed by pure absorption is given by the expression

$$r^{\mu}(\Delta\lambda) = \frac{I^{\mu}_{\text{cont}} - I^{\mu}_{\nu}}{I^{\mu}_{\text{cont}}} = \int_0^{\infty} \frac{1}{\mu} \frac{\kappa_\nu}{\kappa^{\lambda}_{\text{eff}}} \exp\left(-\frac{1}{\mu} \int_0^{\tau_\lambda} \frac{\kappa_\nu}{\kappa^{\lambda}_{\text{eff}}} dt_2 \right) g^{\mu}_{\lambda}(\tau_\lambda)\, d\tau_\lambda , \tag{1}$$

TABLE 1

COMPARISON OF OBSERVED AND PREDICTED GRADIENTS AND BALMER DISCONTINUITIES

Model	Balmer Discontinuity	Gradient	
		λ 4280	λ 3460
Traving (1955)	0.083	0.70	0.34
Model II	.062	.55	.55
τ Scorpii	0.07*	0.68†	0.71†
Mean values:‡			
O9	0.06	0.79	0.64
O9.5–B0	.08	.74	.76
B0.5–B1	0.10	0.72	0.73

* Barbier and Chalonge's data, as corrected by Chalonge and Divan (1952).
† Barbier and Chalonge (1941).
‡ Chalonge and Divan (1952).

TABLE 2

MODEL II FOR THE ATMOSPHERE OF τ SCORPII

θ (1)	x (2)	$\log P_e$ (3)	$\log (\kappa_0+\sigma)$ (4)	θ (1)	x (2)	$\log P_e$ (3)	$\log (\kappa_0+\sigma)$ (4)
0.23	−2.83	1.650	−0.458	0.17	−0.64	3.262	+0.230
.22	−2.15	2.209	− .269	.16	−0.35	3.446	+ .330
.21	−1.60	2.600	− .076	.14	+0.13	3.780	+ .518
.20	−1.30	2.814	+ .022	.12	+0.59	4.037	+ .700
.19	−1.11	2.933	+ .083	0.10	+1.15	4.440	+0.873
0.18	−0.90	3.074	+0.134				

where

$$\mu = \cos \vartheta \; ; \tag{2}$$

and κ_ν = line-absorption coefficient at frequency ν

$\kappa^\lambda_{\text{eff}} = (\kappa^\lambda + \sigma)$ is the effective continuous absorption coefficient, including electron scattering

} per gram of stellar material;

$dt_\lambda = d\tau_\lambda = \kappa^\lambda_{\text{eff}} \rho dh$ is an element of optical depth in the continuum near the line.

Further, we have

$$g^\mu_\lambda(\tau_\lambda) = \frac{\int_{\tau_\lambda}^{\infty} S_\lambda(t_\lambda) \exp(-t_\lambda/\mu)\, dt_\lambda/\mu - S_\lambda(\tau_\lambda) \exp(-\tau_\lambda/\mu)}{\int_0^{\infty} S_\lambda(t_\lambda) \exp(-t_\lambda/\mu)\, dt_\lambda/\mu}, \tag{3}$$

the so-called "weight function." The source function, $S_\lambda(\tau_\lambda)$, is defined in the usual way, viz.,

$$S_\lambda(\tau_\lambda) = \frac{\kappa^\lambda}{\kappa^\lambda + \sigma} B_\lambda(\tau_\lambda) + \frac{\sigma}{\kappa^\lambda + \sigma} \bar{I}_\lambda(\tau_\lambda), \tag{4}$$

where $B_\lambda(\tau_\lambda)$ is the Kirchhoff-Planck function of the local temperature at the depth τ_λ, and

$$\bar{I}_\lambda(\tau_\lambda) = \frac{1}{2} \int_{-1}^{+1} I^\mu_\lambda d\mu$$

is the mean intensity at that depth. We shall carry out the integration in logarithmic scale $\log \tau_\lambda$ rather than in τ_λ directly, so that we do not have to change the step-width (Elste 1955). This change of variable leads to the substitution

$$\log \tau_\lambda = x, \qquad \tau_\lambda = 10^x, \qquad d\tau_\lambda = \frac{10^x}{\text{Mod}}\, dx, \tag{5}$$

where Mod = 0.4343. Then equation (1) becomes

$$r^\mu(\Delta\lambda) = \int_{-\infty}^{+\infty} \frac{1}{\mu} \frac{\kappa_\nu}{\kappa^\lambda_{\text{eff}}} \frac{10^x}{\text{Mod}} \exp\left(- \int_{-\infty}^{x} \frac{1}{\mu} \frac{\kappa_\nu}{\kappa^\lambda_{\text{eff}}} \frac{10^y}{\text{Mod}}\, dy \right) g^\mu_\lambda(x)\, dx. \tag{6}$$

Here the convergence of the integrand is secured by the factor 10^x for the outer layers and by the weight function, $g^\mu_\lambda(x)$, for the deep layers.

Let us now analyze the first part of the integrand according to its functional dependence,

$$\frac{1}{\mu} \frac{\kappa_\nu}{\kappa^\lambda_{\text{eff}}} \frac{10^x}{\text{Mod}} = \frac{1}{\mu} M^* Z \frac{H(v, a)}{\sqrt{\ldots}}. \tag{7}$$

The quantity $\mu = \cos \vartheta$ varies with the position on the stellar disk, M^* is constant, Z is the main depth-dependent part, and $H(v, a)/\sqrt{\ldots}$ depends primarily on the distance $\Delta\lambda$ from the line center. For the moment we shall omit the stimulated emission factor, which will be considered later on. In detail,

$$M^* = \frac{N_i}{N_H} g f_{r,s}\lambda\,[\text{A}] \frac{10^{-8}}{\text{Mod}} \frac{\epsilon^2 \sqrt{\pi}}{m c} \frac{1}{m_H \mu^0} 10^{\theta_0 \Delta\chi} \tag{8}$$

contains all the quantities that are constant for a particular element (N_i/N_H), transition $gf_{r,s}\lambda$[A], $\Delta\chi$, and model atmosphere θ_0, as well as the mathematical and physical con-

stants, including the mean molecular weight of the un-ionized material (with respect to hydrogen),

$$\mu^0 = \frac{\Sigma \mu_i N_i}{N_H}. \tag{9}$$

We transferred the factor $10^{\theta_0 \Delta\chi}$ from the expression for Z over to M^* in order to normalize Z within each ionization stage, which is practical for the use of electronic computing machines and for differential corrections of the model atmosphere. Therefore,

$$Z(x) = \frac{1}{\kappa^{\lambda}_{\text{eff}}} \frac{n_{r,s}}{\Sigma n_r} \frac{10^{x-\theta_0 \Delta\chi}}{g_{r,s}}, \tag{10}$$

where the ratio of the number of absorbing particles to all particles of that element, $n_{r,s}/\Sigma n_r$, is determined by the equations of Boltzmann and Saha. If u_r is the partition function of the rth stage of ionization (the computation of which will be discussed in the next section), we can write

$$\frac{n_{r,s}}{\Sigma n_r} = \frac{n_{r,s}}{n_r/u_r} \frac{1}{u_r(\ldots + n_{r-1}/n_r + 1 + n_{r+1}/n_r + \ldots)}. \tag{11}$$

Let the subscript r denote the most important stage of ionization, and call

$$u_r \frac{n_{r-1}}{n_r} + u_r + u_r \frac{n_{r+1}}{n_r} \equiv U_r. \tag{12}$$

According to Saha's formula, we have

$$\begin{aligned} \log u_r \frac{n_{r-1}}{n_r} &= \log u_{r-1} + \chi_{r-1}\theta - (9.080 - \tfrac{5}{2}\log\theta - \log P_e), \\ \log u_r \frac{n_{r+1}}{n_r} &= \log u_{r+1} - \chi_r \theta + (9.080 - \tfrac{5}{2}\log\theta - \log P_e). \end{aligned} \tag{13}$$

Hence we obtain

$$\begin{aligned} \log Z = x - \log \kappa^{\lambda}_{\text{eff}} - \log U_r \\ + (\chi_{r-1} - \chi_{r-1,s})(\theta - \theta_0) - (9.080 - \tfrac{5}{2}\log\theta - \log P_e) \quad &\text{for } r-1, s, \\ - \chi_{r,s}(\theta - \theta_0) \quad &\text{for } r, s, \\ - (\chi_{r+1,s} + \chi_r)(\theta - \theta_0) + (9.080 - \tfrac{5}{2}\log\theta - \log P_e) \quad &\text{for } r+1, s. \end{aligned} \tag{14}$$

Therefore, we have to define $\Delta\chi$ for the transitions in the three important stages of ionization as follows:

$$\begin{aligned} \Delta\chi &= (\chi_{r-1} - \chi_{r-1,s}) \quad &\text{for } r-1, s \\ &= -\chi_{r,s} \quad &\text{for } r, s \\ &= -(\chi_{r+1,s} + \chi_r) \quad &\text{for } r+1, s. \end{aligned} \tag{15}$$

As we shall see in the examples in Section V, $\log Z$ behaves as a function of x quite a bit differently for different elements, ionization stages, and excitations.

The last expression in equation (7) is

$$\frac{H(v, a)}{\sqrt{\ldots}} = \frac{1}{\sqrt{\ldots}} \frac{a}{\pi} \int_{-\infty}^{+\infty} \frac{\exp(-y^2)}{a^2 + (v-y)^2}\, dy . \tag{16}$$

This is the wave-length-dependent part of the line-absorption coefficient, containing thermal, natural, and collisional broadening. Its slight dependence on depth lies in

$$v = \frac{\Delta\lambda}{\Delta\lambda_D} = \frac{\Delta\lambda}{\lambda} \frac{c}{\sqrt{\ldots}} \quad \text{and} \quad a = \frac{\Gamma}{4\pi} \frac{\lambda}{\sqrt{\ldots}}, \tag{17}$$

with the abbreviation

$$\sqrt{\ldots} = \sqrt{(\xi_{\text{th}}^2 + \xi_{\text{turb}}^2)} . \tag{18}$$

Here ξ_{th} is the thermal velocity and ξ_{turb} the most probable velocity of the microturbulence (i.e., the eddy size is smaller than the thickness of the absorbing layer). If ξ_{th} and ξ_{turb} are both expressed in kilometers per second, then

$$\xi_{\text{th}}^2 = \frac{2RT}{\mu_{\text{element}}} = \frac{83.83}{\mu_{\text{element}}} \frac{1}{\theta} . \tag{19}$$

Our equation (6) for the line depth in intensity can now be written thus:

$$r^{\mu}(\Delta\lambda) = \int_{-\infty}^{+\infty} \frac{M^*}{\mu} \frac{Z}{\sqrt{\ldots}} H(v, a) \exp\left[-\int_{-\infty}^{x} \frac{M^*}{\mu} \frac{Z}{\sqrt{\ldots}} H(v, a)\, dy \right] \times g_{\lambda}^{\mu}(x)\, dx . \tag{20}$$

In order to get the equivalent width,

$$W_{\lambda}^{\mu} = \int_{-\infty}^{+\infty} \frac{I_{\text{cont}}^{\mu} - I_{\nu}^{\mu}}{I_{\text{cont}}^{\mu}}\, d(\Delta\lambda) , \tag{21}$$

we have to integrate equation (20) over the wave-length scale $d(\Delta\lambda) \equiv \Delta\lambda_D dv$. A further division by λ leads to the quantity $W_{\lambda}^{\mu}/\lambda$, whose logarithm is the ordinate of the curve of growth. The right-hand side of equation (20) therefore has to be multiplied by $\Delta\lambda_D/\lambda = \sqrt{\ldots}/c$, which cancels with the first Doppler root and leaves only a division by c. The integration over dv can now be simplified by using the fact that $H(v, a)/\sqrt{\ldots}$ varies only slowly with depth in the atmosphere and can therefore be placed in front of the integral in the exponent without introducing a serious error:

$$\frac{W_{\lambda}^{\mu}}{\lambda} = \int_{-\infty}^{+\infty} \frac{M^*}{c\mu} Z(x) \int_{-\infty}^{+\infty} H(v, a) \exp\left[-\frac{H(v, a)}{\sqrt{\ldots}} \int_{-\infty}^{x} \frac{M^*}{\mu} Z(y)\, dy \right] \times dv\, g_{\lambda}^{\mu}(x)\, dx . \tag{22}$$

If we call

$$\frac{M^*}{\mu\sqrt{\ldots}} \int_{-\infty}^{x} Z(y)\, dy = \frac{Y}{\mu}, \tag{23}$$

the function

$$\int_0^{\infty} H(v, a) \exp\left[-H(v, a) \frac{Y}{\mu} \right] dv$$

is Pecker's *saturation function*, which approaches $\sqrt{\pi}/2$ for $\lim Y \to 0$. Introducing the normalized saturation function,

$$\frac{2}{\sqrt{\pi}} \int_0^{\infty} H(v, a) \exp\left[-H(v, a) \frac{Y}{\mu} \right] dv = \Psi\left(\frac{Y}{\mu}, a \right), \tag{24}$$

which differs from Pecker's notation by the normalization factor $2/\sqrt{\pi}$, we can write

$$\frac{W_\lambda^\mu}{\lambda} = \int_{-\infty}^{+\infty} \frac{M^*}{\mu} \frac{\sqrt{\pi}}{c} Z(x)\, \Psi\left(\frac{Y}{\mu}, a\right) g_\lambda^\mu(x)\, dx \tag{25}$$

and call it $\mathfrak{L}_\lambda^\mu M/\mu$ in the case of medium-strong lines and $L_\lambda^\mu M/\mu$ in the ideal case of weak lines, i.e., if $\Psi(Y/\mu, a) \equiv 1$. Note that L_λ^μ itself is independent of M, while $\mathfrak{L}_\lambda^\mu$ depends on the strength of the line. Both quantities vary with the excitation conditions, the wave length, and the atmospheric model used.

Our constants now are defined as follows:

$$M \equiv \frac{M^* \sqrt{\pi}}{c} = \frac{N_i}{N_H}\, g f_{r,\,s}\lambda\,[\mathrm{A}]\; 10^{\theta_0 \Delta\chi} \frac{\pi\epsilon^2}{m c^2} \frac{10^{-8}}{\mathrm{Mod}} \frac{1}{m_H \mu^0}, \tag{26}$$

$$k = \frac{\pi\epsilon^2}{m c^2} \frac{10^{-8}}{\mathrm{Mod}} \frac{1}{m_H \mu^0}, \tag{27}$$

$$\log M = \log \frac{N_i}{N_H} + \log\, g f_{r,\,s}\lambda\,[\mathrm{A}]\; k + \theta_0 \Delta\chi\,. \tag{28}$$

Therefore, we have to write

$$\frac{Y}{\mu} = \frac{M}{\mu} \frac{c}{\sqrt{\pi}} \frac{1}{\sqrt{\ldots}} \int_{-\infty}^{x} Z(y)\, dy\,, \tag{29}$$

with c and $\sqrt{\ldots}$ both in kilometers per second. The formulae for the equivalent width in flux can be derived by integrating the formulae for intensities over the disk of the star according to

$$\pi F = 2\pi \int_0^{+1} I^\mu \mu d\mu\,; \tag{30}$$

hence we obtain

$$\begin{aligned} \frac{W_\lambda}{\lambda} &= \frac{1}{\lambda} \int_{-\infty}^{+\infty} \frac{F_{\mathrm{cont}} - F_\nu}{F_{\mathrm{cont}}}\, d\Delta\lambda \\ &= \frac{1}{\lambda} \int_{-\infty}^{+\infty} \int_0^{+1} \frac{I^\mu_{\mathrm{cont}} - I^\mu_\nu}{I^\mu_{\mathrm{cont}}} \frac{I^\mu_{\mathrm{cont}}}{F_{\mathrm{cont}}/2}\, \mu d\mu d\Delta\lambda\,. \end{aligned} \tag{31}$$

Changing the order of integration and using equation (21), we get

$$\frac{W_\lambda}{\lambda} = \int_0^1 \frac{W_\lambda^\mu}{\lambda} \frac{I^\mu_{\mathrm{cont}}}{F_{\mathrm{cont}}/2}\, \mu d\mu\,. \tag{32}$$

Notice that $I^\mu_{\mathrm{cont}}(\tau_\lambda = 0)$ is the quantity which appears in the denominator of the weight function, equation (3),

$$g_\lambda^\mu(\tau_\lambda) = \frac{\int_{\tau_\lambda}^{\infty} S_\lambda(t_\lambda) \exp(-t_\lambda/\mu)\, dt_\lambda/\mu - S_\lambda(\tau_\lambda) \exp(-\tau_\lambda/\mu)}{I^\mu_{\mathrm{cont}}(\tau_\lambda = 0)}. \tag{33}$$

Before we actually carry out the integration of equation (32) over μ, we shall write the weight function in a more practical form, which will also be useful for its evaluation:

$$I^\mu_{\mathrm{cont}}(\tau_\lambda = 0)\; g_\lambda^\mu(\tau_\lambda) = \int_{\tau_\lambda}^{\infty} \frac{dS_\lambda(t_\lambda)}{dt_\lambda} \exp\left(-\frac{t_\lambda}{\mu}\right) dt_\lambda\,. \tag{34}$$

Using equations (25) and (34), we obtain, from equation (32),

$$\frac{W_\lambda}{\lambda}=\frac{1}{F_{\text{cont}}/2}\int_0^1 \mu d\mu \int_{-\infty}^{+\infty} dx\,\frac{MZ}{\mu}\Psi\left(\frac{Y}{\mu},a\right)\int_{\tau_\lambda}^{\infty} dt_\lambda \frac{dS_\lambda(t_\lambda)}{dt_\lambda}\exp\left(-\frac{t_\lambda}{\mu}\right). \quad (35)$$

Let us now change the order of integration, integrating successively over μ, t_λ, and finally x, viz.,

$$\frac{W_\lambda}{\lambda}=\frac{2}{F_{\text{cont}}}\int_{-\infty}^{+\infty} dx MZ\int_{\tau_\lambda}^{\infty} dt_\lambda \frac{dS_\lambda(t_\lambda)}{dt_\lambda}\int_0^1 d\mu\Psi\left(\frac{Y}{\mu},a\right)\exp\left(-\frac{t_\lambda}{\mu}\right). \quad (36)$$

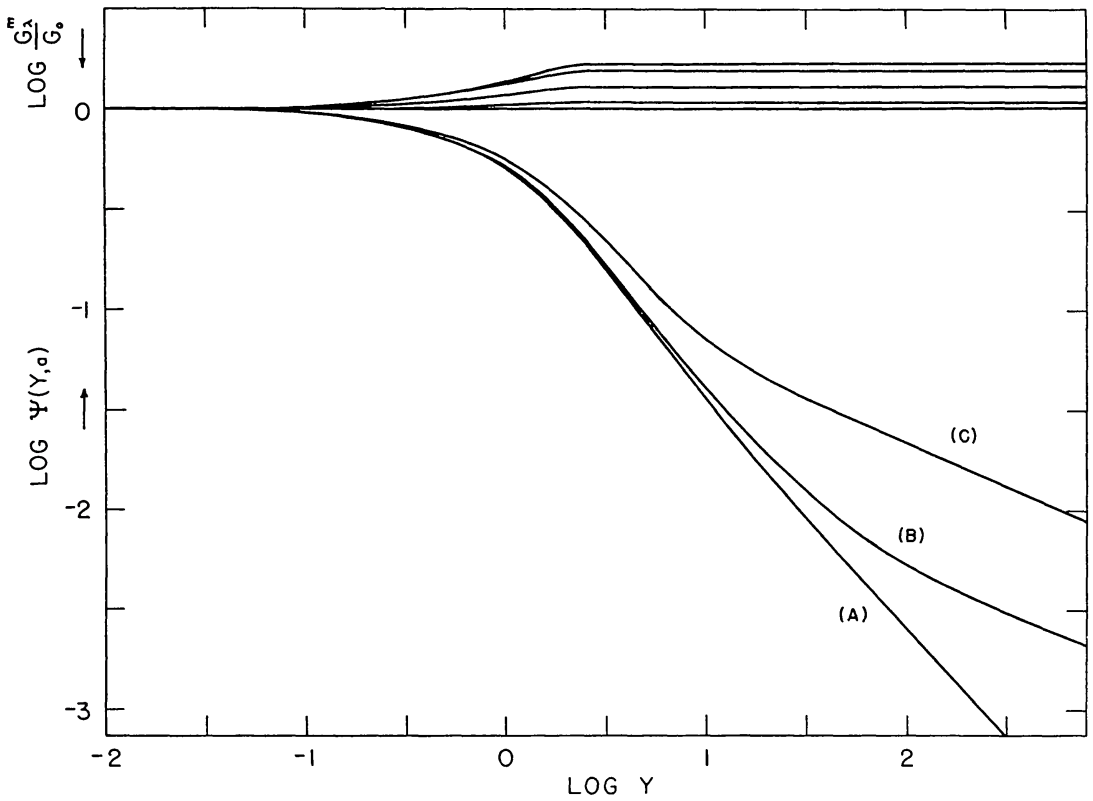

FIG. 1.—The saturation function. The saturation function, $\Psi(Y, a)$, defined by equation (24) is plotted as a function of Y (eq. [45]) with the parameter $\log a = -\infty$ (pure Doppler broadening, curve A), -2 (curve B), and -1 (curve C). The four curves at the top of the graph give the saturation weight (eqs. [40], [41], and [42]) plotted as a function of Y and $x = -2, -1, 0$, and $+1$ for the model atmosphere of τ Scorpii. The curve for $x = -2$ falls at top of diagram.

An examination of Figure 1, which exhibits the saturation function in logarithmic form, shows that Ψ can be approximated over small regions in Y/μ by a formula of the type

$$\log\Psi=-m\log\frac{Y}{\mu}+\text{const.} \qquad \text{with} \qquad 0\leq m\leq +1.25. \quad (37)$$

That is, Ψ contains one factor depending on Y and another depending on μ, viz.,

$$\Psi\left(\frac{Y}{\mu},a\right)\simeq\Psi(Y,a)_{\mu=1}\mu^m. \quad (38)$$

Therefore, we can carry out the essential integration over the disk and find

$$\int_0^1 \exp\left(-\frac{t_\lambda}{\mu}\right) \mu^{+m} d\mu = E_{m+2}(t_\lambda) . \tag{39}$$

Originally, the exponential integral was defined only for integers. Pecker (1953) discussed the analytic expansion and computed some of the useful functions for values of $m = \frac{1}{2}, \frac{3}{2}, \ldots$. For weak lines $\Psi = 1$, so that $m = 0$. We now define the weight functions for the flux as

$$G_\lambda^0(\tau_\lambda) = \frac{2}{F_{\text{cont}}} \int_{\tau_\lambda}^{\infty} \frac{dS_\lambda(t_\lambda)}{dt_\lambda} E_2(t_\lambda)\, dt_\lambda . \tag{40}$$

If we want to compute actual equivalent widths for medium-strong lines, we have to use other weight functions, according to the logarithmic gradient m, which depends on Y:

$$G_\lambda^m(\tau_\lambda) = \frac{2}{F_{\text{cont}}} \int_{\tau_\lambda}^{\infty} \frac{dS_\lambda(t_\lambda)}{dt_\lambda} E_{m+2}(t_\lambda)\, dt_\lambda . \tag{41}$$

Let us call the ratio by which the weight function G_λ^0 has to be multiplied in order to take care of the gradient of the saturation function the *saturation weight with respect to* μ,

$$\frac{G_\lambda^m(\tau_\lambda)}{G_\lambda^0(\tau_\lambda)} . \tag{42}$$

Here m is a known function of Y. Ratio (42) depends on m and τ_λ and the particular model atmosphere. With these definitions, our equations for the equivalent width of weak lines and of medium-strong lines become

$$\frac{W_\lambda}{\lambda} = \int_{-\infty}^{+\infty} MZ(x)\, G_\lambda^0(x)\, dx = ML_\lambda \tag{43}$$

and

$$\frac{W_\lambda}{\lambda} = \int_{-\infty}^{+\infty} MZ(x)\, \Psi(Y, a) \frac{G_\lambda^m(x)}{G_\lambda^0(x)} G_\lambda^0(x)\, dx = M\mathfrak{L}_\lambda , \tag{44}$$

with

$$Y = M \frac{c}{\sqrt{\pi}} \frac{1}{\sqrt{\ldots}} \int_{-\infty}^{x} Z(y)\, dy . \tag{45}$$

In order to carry out the computations efficiently, it is best to use as the variable of integration the logarithm of the optical depth at one standard wave length, λ_0, i.e., $\log \tau_{\lambda_0}$. This arrangement has the advantage that in the expression for Z we have only one temperature and pressure distribution to consider when computing $n_{r,s}/\Sigma n_r$. The connection between the optical depths at different wave lengths must still be considered for the weight functions. The weight function for each different wave length has to be computed in the optical-depth scale of the particular wave length under consideration and then transformed to the $\log \tau_{\lambda_0}$ scale by using the relation between the $\log \tau_\lambda$ scales,

$$\tau_\lambda = \int_0^{\tau_{\lambda_0}} \frac{\kappa_{\text{eff}}^{\lambda}}{\kappa_{\text{eff}}^{\lambda_0}} dt_{\lambda_0} , \tag{46}$$

which is determined by the model (τ_{λ_0} θ, log P_e). The computation of the weight functions is based on the given source functions $S_\lambda(\tau_\lambda)$ and will be carried out also on a logarithmic scale. Using a linear approximation of the source function for each step in log τ_λ, we find, from equation (41),

$$G_\lambda^m (\log \tau_\lambda) = \frac{2}{F_\lambda (0)} \sum_{\log \tau_\lambda = 1}^{\log \tau_\lambda} \frac{\Delta S_\lambda (\log \tau_\lambda)}{\Delta \log \tau_\lambda} \int_{\log \tau_\lambda}^{\log \tau_\lambda + \Delta \log \tau_\lambda} E_{m+2} (\log t_\lambda)\, d \log t_\lambda , \quad (47)$$

summing up from deeper layers outward. For $-3 \leq \log \tau_\lambda \leq +1$ and $\Delta \log \tau_\lambda = 0.2$, the functions

$$\frac{1}{0.2} \int_{\log \tau_\lambda}^{\log \tau_\lambda + 0.2} E_{m+2} (\log t_\lambda)\, d \log t_\lambda \qquad \text{for} \qquad m = 0, \tfrac{1}{2}, 1 \quad (48)$$

are given in the appendix as Table A1. In the discussion of the hot atmospheres of early-type stars the factor of stimulated emission,

$$(1 - 10^{-\chi_\lambda \theta}) \qquad \text{with} \qquad \chi_\lambda = \frac{12395}{\lambda\ [\text{A}]} \quad (49)$$

belonging to $\kappa_\nu / \kappa_{\text{eff}}^\lambda$, has to be taken into account. Because of its wave-length dependence, it is convenient to treat this function along with the weight function. This stimulated emission factor has also to be included in the formula for Y. Therefore, our final equations are

$$\frac{W_\lambda}{\lambda} = \int_{-\infty}^{+\infty} MZ\,(x)\, G_\lambda^0\,(x)\,(1 - 10^{-\chi_\lambda \theta})\, dx = ML_\lambda^* , \quad (50)$$

$$\frac{W_\lambda}{\lambda} = \int_{-\infty}^{+\infty} MZ\,(x)\, \Psi\,(Y, a)\, \frac{G_\lambda^m\,(x)}{G_\lambda^0\,(x)}\, G_\lambda^0\,(x)\,(1 - 10^{-\chi_\lambda \theta})\, dx = M\mathfrak{L}_\lambda^* , \quad (51)$$

with

$$Y = M \frac{c}{\sqrt{\pi}} \frac{1}{\sqrt{\ldots}} \int_{-\infty}^{x} Z\,(y)\,(1 - 10^{-\chi_\lambda \theta})\, dy \quad (52)$$

and

$$\log M = \log \frac{N_i}{N_H} + \log\, g f_{r,\,s} \lambda\ [\text{A}]\ k + \theta_0 \Delta\chi , \quad (53)$$

$$\log k = 3.8405 , \qquad \log \frac{c}{\sqrt{\pi}} = +5.2282 . \quad (54)$$

Repeating equation (14), we obtain

$$\begin{aligned} \log Z = {} & x - \log\, \kappa_{\text{eff}}^{\lambda_0} - \log\, U_r \\ & + (\chi_{r-1} - \chi_{r-1,\,s})(\theta - \theta_0) - (9.080 - \tfrac{5}{2} \log \theta - \log P\epsilon) \qquad \text{for} \qquad r-1,\ s , \\ & \qquad - \chi_{r,\,s} (\theta - \theta_0) \qquad \text{for} \qquad r,\ s , \\ & - (\chi_{r+1,\,s} + \chi_r)(\theta - \theta_0) + (9.080 - \tfrac{5}{2} \log \theta - \log P_\epsilon) \qquad \text{for} \qquad r+1,\ s . \end{aligned} \quad (55)$$

IV. CALCULATION OF PARTITION FUNCTIONS

In the calculation of the ionization equilibrium it has been necessary to compute the partition functions of those elements whose lines are represented in the spectrum. These partition functions will depend on both the temperature and the density, since the latter determines the number of levels that may be occupied.

In the calculations for carbon, nitrogen, oxygen, and silicon, which were carried out first, we simply used the levels listed in Miss Moore's tables and did not introduce the pressure effects which become important for some ions at high temperatures. The density effects would become important for, e.g., C II or O II at large optical depths, but in these regions the amounts of C II or O II as compared with C III or O III is negligibly small. Calculations of the density effects have been carried out for neon, aluminum, and magnesium. They are appreciable for the metals but unimportant for neon.

The calculations are carried out with the aid of formulae very similar to those employed by Claas (1951) and more recently by Pecker's project. We write

$$u = \sum_{1}^{\infty} g_n p_n \exp\left(-\frac{\chi_n}{kT}\right) = u_0 + u_1, \tag{56}$$

where

$$u_0 = \sum_{1}^{m-1} g_n p_n \exp\left(-\frac{\chi_n}{kT}\right) \tag{57}$$

is computed with the levels obtained from Miss Moore's term table (1949). Here g_n is the statistical weight, while p_n expresses the likelihood that the level n is actually occupied. For low-lying levels $p_n = 1$, but, as the orbital radius of the level n approaches the mean interatomic distance, p_n approaches zero. The term

$$u_1 = \sum_{m}^{\infty} g_n p_n \exp\left(-\frac{\chi_n}{kT}\right) \tag{58}$$

is computed on the assumption that the highest levels can be regarded as strictly hydrogenic. For the levels beyond those given in Miss Moore's table and up to and including $n = 15$ we compute

$$u_1' = \sum_{m}^{n=15} p_n \rho n^2 \exp\left(-\frac{\chi_n}{kT}\right). \tag{59}$$

Here ρ is the multiplicity of the spectrum, and the p_n's are evaluated for each level according to the theory by Unsöld, viz.,

$$p_n = \exp\left[-C(Z) P_e n^6 \theta\right], \tag{60}$$

where $C(Z)$ is a numerical constant whose value depends on the charge on the nucleus. Finally, for levels 16 and higher, χ_n may be replaced by the ionization potential χ, and we may compute

$$u_1'' = 10^{-\chi\theta} \sum_{n=16}^{\infty} \rho n^2 \exp\left[-C(Z) P_e n^6 \theta\right] \sim \rho 10^{-\chi\theta} \int_{16}^{\infty} x^2 \exp\left[-C(Z) P_e x^6 \theta\right] dx. \tag{61}$$

If we put

$$x = y^{1/3} \left[C(Z) P_e \theta\right]^{-1/6} \tag{62}$$

and

$$y_1 = n^3 \sqrt{[C\,(Z)\,P_e\theta]}\ ,$$

we find

$$u_1'' = \frac{\rho 10^{-\chi\theta}}{3\sqrt{[C\,(Z)\,P_e\theta]}} \int_{y_1}^{\infty} \exp\,(-y^2)\,dy \tag{63}$$

and

$$u_1 = u_1' + u_1''\ . \tag{64}$$

Table 3*a* gives the partition functions for silicon and for oxygen, carbon, and nitrogen, while Table 3*b* gives the data for magnesium, aluminum, and neon in the ionization stages of interest for selected values of θ and log P_e. Similar calculations have also been carried out for helium (Jugaku and Elste 1957) with the aid of the IBM 650 computer and the MITILAC interpretive routine.

TABLE 3*a*

PARTITION FUNCTIONS FOR OXYGEN, CARBON, NITROGEN, AND SILICON

θ	Oxygen			Carbon			Nitrogen			Silicon	
	u_{II}	u_{III}	u_{IV}	u_{II}	u_{III}	u_{IV}	u_{II}	u_{III}	u_{IV}	u_{III}	u_{IV}
0.23....	6.15	10.49	6.12	6.78	1.30	2.08	11.30	6.30	1.11	1.30	2.06
.22....	6.34	10.60	6.16	6.90	1.35	2.11	11.40	6.38	1.12	1.36	2.07
.21....	6.54	10.72	6.20	7.05	1.41	2.13	11.52	6.46	1.16	1.42	2.08
.20....	6.75	10.85	6.25	7.23	1.48	2.15	11.62	6.54	1.20	1.49	2.10
.19....	7.00	11.00	6.31	7.41	1.56	2.18	11.85	6.61	1.24	1.58	2.12
.18....	7.30	11.18	6.38	7.59	1.65	2.21	12.07	6.71	1.29	1.68	2.16
.17....	7.61	11.36	6.46	7.86	1.77	2.26	12.3	6.82	1.36	1.79	2.19
.16....	7.96	11.56	6.55	8.18	1.91	2.30	12.7	6.98	1.43	1.93	2.24
.14....	8.82	12.04	6.78	9.25	2.23	2.45	13.6	7.44	1.63	2.40	2.36
.12....	10.07	12.72	7.17	11.5	2.73	2.69	14.5	8.17	1.95	3.20	2.58
0.10....	11.7	13.75	7.93	17.3	3.53	2.96	16.3	9.17	2.37	4.45	2.93

TABLE 3*b*

PARTITION FUNCTIONS FOR NEON, MAGNESIUM, AND ALUMINUM

	Mg II	Mg III	Al II	Al III	Ne I	Ne II	Ne III
θ=0.10, log P_e=2.....	1640	1.002	1400	169	178	18.9	11.9
θ=0.10, log P_e=3.....	505	1.00	453	57	50	10.2	11.7
θ=0.10, log P_e=4.....	148	1.00	154	21.0	14.7	7.5	11.6
θ=0.14, log P_e=2.....	349	1.00	213	13.1	21.5	6.26	10.9
θ=0.14, log P_e=3.....	110	1.00	72	6.14	6.75	6.09	10.9
θ=0.14, log P_e=4.....	34	1.00	27.1	3.95	2.93	6.04	10.9
θ=0.18, log P_e=2.....	79.6	1.00	35.4	3.07	3.46	6.01	10.4
θ=0.18, log P_e=3.....	26.7	1.00	13.4	2.63	1.68	6.00	10.4
θ=0.18, log P_e=4.....	10.0	1.00	6.5	2.49	1.25	6.00	10.4
θ=0.23, log P_e=2.....	14.7	1.00	5.26	2.21	1.18	6.00	9.94
θ=0.23, log P_e=3.....	6.4	1.00	3.03	2.19	1.05	6.00	9.94
θ=0.23, log P_e=4.....	3.8	1.00	2.32	2.19	1.02	6.00	9.94

V. THE APPLICATION OF THE THEORY

We shall now describe how the formulae collected in Section III may be used in the numerical calculation of line intensities in the stellar spectrum. The revised Traving (1955) model, with log $g = 4.30$, has a lower electron pressure than the original Traving model at corresponding optical depths, since it involves a lower surface gravity. We have recomputed the following quantities for wave lengths λλ 3272, 3650, 4000, and 4600:

1. The effective absorption coefficient $\kappa_\lambda + \sigma$, using the Kyoto tables (Ueno, Saito, and Jugaku 1954).
2. The relation between log τ_λ and log τ_{λ_0}, by equation (46).

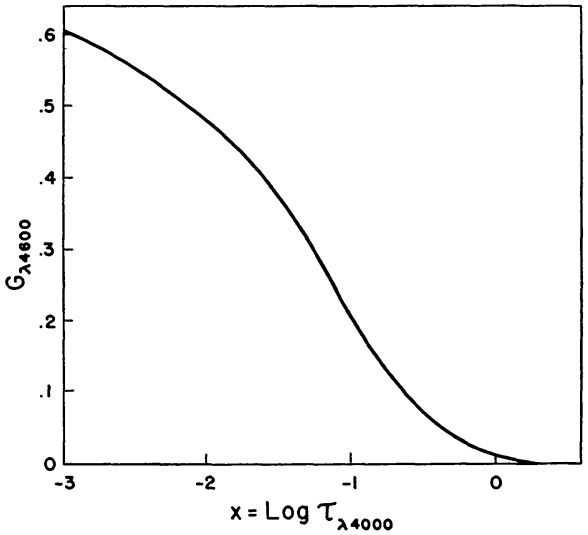

FIG. 2.—The weight function $G^*_{\lambda\,4600}(x)$. The weight function as defined by equation (40) is multiplied by the stimulated emission factor (eq. [49]) to give $G^0_{\lambda\,4600}(x)(1 - 10^{-\theta x_\lambda}) = G^*_{\lambda\,4600}(x)$. The abscissa is $x = \log \tau_{\lambda_0}$, where $\lambda_0 = 4000$ A.

3. The source function S_λ (log τ_λ), defined by equation (4), using Strömgren's iteration procedure, which is described, for example, by Underhill (1950) and Aller (1953).
4. The monochromatic flux at the surface, $F_\lambda(0)$, with the aid of a Gaussian quadrature formula suggested by Strömgren (see, e.g., Chandrasekhar 1950, chap. ii; Aller 1953, chap. 7).

The computation of the weight functions (eq. [3]) as functions of log τ_λ may be carried out by using equation (47) and Appendix Table A1. For other than the standard wave length, $\lambda_0 = 4000$ A, we plotted the functions G^0_λ (log τ_λ) on a scale $x = \log \tau_{\lambda_0}$, making use of the relation between log τ_λ and log τ_{λ_0}. We obtained $G^0_\lambda(x)$ as a function of $x = \log \tau_{\lambda_0}$ in steps of 0.2 by graphical interpolation. Figure 2 gives $G^*_{\lambda\,4600}(x)$ as an example. Next, following equation (49), we form and tabulate the product

$$G^0_\lambda(x)\,(1 - 10^{-\theta x_\lambda}) = G^*_\lambda(x)\,.$$

Before starting the actual computation of log U_r (eq. [10]), we first plotted $\theta = 5040/T$ as a function of $x = \log \tau_{\lambda_0}$ and chose our reference θ_0 as 0.18, a convenient value in the range $-0.5 < x < 0$. To within the limits of "astrophysical accuracy" as imposed by our model atmosphere, it is sufficient to compute log U_r and log Z for about ten properly chosen values of θ throughout the atmosphere and to use both numerical and graphical methods of integration. For each θ we compute the quantity $(9.080 - \frac{5}{2} \log \theta - \log P_e)$ that appears in equations (13) and (14). For each observed stage of

ionization of an element, we have to know for which excitations the log L^*_λ has to be computed in order to cover the range of the observed transitions. Therefore, we prepared lists giving, in successive columns, the multiplet, J-values, the wave length λ, log $gf_{r,s}$, $\Delta\chi$, log C, W_λ, and log W_λ/λ, out of which we selected some three values of $\Delta\chi$. An example of such a list for Si III in τ Scorpii is given in Table 4, the three values $\Delta\chi$ chosen are 7.60, 11.84, and 14.54 ev (also $\chi_{III} = 33.46$ ev).

In computing log U_r and log Z for silicon, we chose $r = 4$ as being appropriate for the most important ionization stage of this element in the atmosphere of τ Scorpii. The computations were then carried out according to equations (12), (13), (14), and (15) for $\theta = 0.10$, 0.12, 0.14, 0.16, 0.17, 0.18, 0.19, 0.20, 0.21, 0.22, and 0.23, and log Z was

TABLE 4

DATA FOR OBSERVED LINES OF SILICON IN τ SCORPII

MULTIPLET (1)	$J'-J$ (2)	λ (3)	log gf (4)	$\Delta\chi$ (5)	log C (6)	W_λ (7)	log W_λ/λ (8)
			Si III				
4^3S-4^3P	1–2	4553	+0.314	14.46	0.626	112	0.391–5
	1–1	4568	+ .087	.....	.398	97	.328–5
	1–0	4575	− .383	.....	.927–1	63	.140–5
4^3P-4^3D	2–	3807	+ .704	11.74	.562	75	.295–5
	1–	3796	+ .434	11.75	.293	24	.802–6
	0–1	3791	+ .084	11.75	.944–1	44	.065–5
$4^1P^0-4^1D$	1–2	3590	+ .557	11.58	.397	32	.950–6
4^3F-5^3G	4–	4829	+ .932	7.49	.853–1	63	.116–5
	3–	4820	+ .822	7.50	.746–1	49	.007–5
	2–3	4813	+0.702	7.50	0.626–1	31:	0.81–6
			Si IV				
			$\chi_{r,s}$				
4^2S-4^2P	$\frac{1}{2}-\frac{3}{2}$	4089	+0.19	24.04	1.403	136	0.522–5
	$\frac{1}{2}-\frac{1}{2}$	4116	−0.11	24.04	1.096	117	.454–5
4^2D-5^2P	$\frac{5}{2}-\frac{3}{2}$	3762	+0.26	30.99	0.396	60	.203–5
	$\frac{3}{2}-\frac{1}{2}$	3773	0.0	30.99	0.132	15	.600–6
5^2D-6^2F	.....	4212	+0.81	36.13	0.988–1	44	.020–5
5^2F-6^2G	.....	4631	+1.18	36.41	0.175	55	.075–5
5^2G-6^2H	.....	4654	+1.37	36.42	0.358	72	0.190–5

plotted as a function of $x = \log \tau_{\lambda_0}$. Figure 3 represents our example for Si III. Using these graphs, we read off the values Z themselves in steps of $\Delta x = 0.2$ with the aid of a logarithmic scale. Then we multiply them by the weight functions $G^*_\lambda(x)$ and add them up. This gives, following equation (50), the main part of the integral L^*_λ for each $\Delta\chi$. The functions $Z(x)\, G^*_\lambda(x)$ under the integral sign, the so-called "contribution functions," approach zero in both directions to $-\infty$ and $+\infty$, as shown in Figure 4. While in the outer layers the term 10^x, included in Z, produces the convergence, in the deeper layers the fast-decreasing weight function does it. The integrals from $-\infty$ to the point x_0, where we started the stepwise integration, were estimated by the formula

$$\frac{1}{\Delta x}\int_{-\infty}^{x_0} Z\,(x)\, G^*_\lambda\,(x)\, dx = \frac{\text{Mod}}{0.2}\, Z\,(x_0)\, G^*_\lambda\,(x_0) \qquad (65)$$

and taken into account when necessary.

Next, with $\Delta\chi$ as the parameter, we draw graphs giving log L^*_λ as a function of λ in order to interpolate log L^*_λ for the wave-length and excitation difference $\Delta\chi$ of each line in our list. The abscissa of the curve of growth is then obtained as follows:

$$\log C = \log \lambda g f_{r,s} k + \Delta\chi\, \theta_0 + \log L^*_\lambda\ (\Delta\chi)\ . \tag{66}$$

The empirical curve of growth, i.e., the plot of log W_λ/λ versus log C, now permits an estimation of the probable position of the 45° line that corresponds to a line of "zero saturation." To calculate points of the threoretical curve, i.e., predicted values of log W_λ/λ including the proper saturation, it is necessary to know log M (eqs. [52] and [53]).

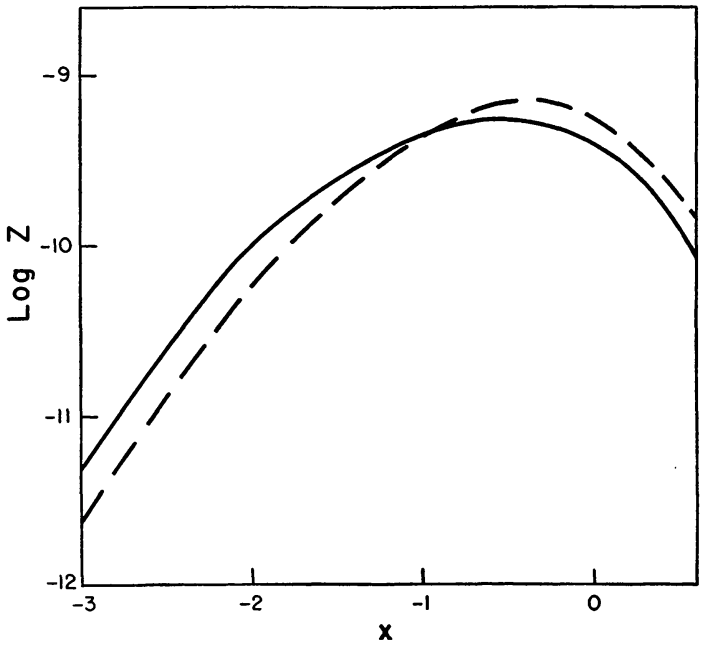

FIG. 3.—The function $Z(x)$ for Si III. The ordinate is log $Z(x)$, the abscissa is $x = \log \tau_{\lambda_0}$. The solid curve gives log Z for $\Delta\chi = 11.84$ ev; the dashed curve, log Z for 7.60 ev.

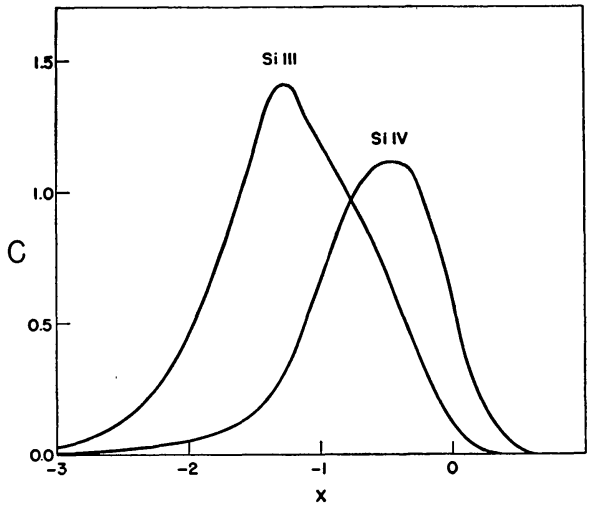

FIG. 4.—The contribution functions for Si III and Si IV. The contribution function for weak lines $Z(x)G^0_\lambda(x)(1 - 10^{-\theta\chi_\lambda})$ is plotted for λ 4000 A, Si III ($\Delta\chi = 11.84$ ev), and Si IV ($\Delta\chi = -23.95$ ev). The unit of the ordinate is 10^{-10} for Si III and 10^{-2} for Si IV.

We illustrate this problem in the case of Si IV with two lines near λ 4600, $\chi_{r,\,s} = 36.26$ ev, and log $C = 0.20$ and 0.36. At log $C = 0.20$, we might estimate that the 45° line would go through log $W_\lambda/\lambda = -4.45$. Hence, according to equation (50), we have

$$\log M = \log \frac{W_\lambda}{\lambda} - \log L_\lambda^* = -2.50\,. \tag{67}$$

The logarithm of the integral

$$\int_{-\infty}^{x} Z\,(x)\,(1 - 10^{-\theta\chi_\lambda})\,dx\,,$$

which is included in Y (eq. [52]) can be obtained most conveniently by a nomographical method (see Appendix II) on a graph giving log $Z(x)\,(1 - 10^{-\theta\chi_\lambda})$ as a function of $x = \log \tau_{\lambda_0}$. Since there appears to be no evidence of microturbulence in τ Scorpii, we have taken into account only the thermal part of the Doppler root, $\sqrt{(83.83/\mu_i\theta)}$. From equation (53) we have

$$\log Y = \log M + \log \frac{C}{\sqrt{\pi}} + \tfrac{1}{2}\log \frac{\mu_i}{83.83} + \log \sqrt{\theta} \int_{-\infty}^{x} Z\,(x)\,(1 - 10^{-\theta\chi_\lambda})\,dx\,, \tag{68}$$

whose zero point falls at

$$\log \sqrt{\theta} \int_{-\infty}^{x} Z\,(x)\,(1 - 10^{-\theta\chi_\lambda})\,dx = -\left(\log M + \log \frac{C}{\sqrt{\pi}} + \tfrac{1}{2}\log \frac{\mu_i}{83.83}\right). \tag{69}$$

In the present example for Si IV this is equal to 2.49.

In order to apply the saturation function $\Psi(Y, a)$ and the saturation weight $G_\lambda^m(x)/G_\lambda^0(x)$ simultaneously, we have appended to the graph that gives log Ψ as a function of log Y a further family of curves, giving log $G_\lambda^m(x)/G_\lambda^0(x)$ as a function of log Y because m depends on Y with x as a parameter. The quantity log $G_\lambda^m(x)/G_\lambda^0(x)$ was computed for $x = -3$, -2.5, -2, -1.5, -1, -0.5, 0, $+0.5$, and $+1$ with the aid of equation (47) and Appendix Table A1, but only for the wave length λ_0, since it is farily insensitive to wave length.

We evaluated the function

$$\log Z\,(x)\,(1 - 10^{-\theta\chi_\lambda})\,\Psi\,(Y,\,a)\,\frac{G_\lambda^m\,(x)}{G_\lambda^0\,(x)}$$

on the graph, showing

$$\log Z\,(x)\,(1 - 10^{-\theta\chi_\lambda}) \qquad \text{and} \qquad \log \sqrt{\theta} \int_{-\infty}^{x} Z\,(x)\,(1 - 10^{-\theta\chi_\lambda})\,dx$$

as functions of $x = \log \tau_{\lambda_0}$. This graph should have the same scale units as the one showing the saturation function, log $\Psi(Y, a)$, versus log Y. (A scale of 10 cm equal to one power of 10 was actually used.)

Figure 5 illustrates our procedure. At the points $x = \log \tau_{\lambda_0}$ where we wish to assess the saturation, we place the log Ψ − log Y graph so that its log Y scale runs in the direction of

$$\log \sqrt{\theta} \int_{-\infty}^{x} Z\,(x)\,(1 - 10^{-\theta\chi_\lambda})\,dx\,,$$

with the zero point (log $Y = 0$), which can be determined by equation (69) and is 2.49 in our illustrative example. Now the local value of the curve

$$\log \sqrt{\theta} \int_{-\infty}^{x} Z\,(x)\,(1 - 10^{-\theta\chi_\lambda})\,dx$$

determines the log Y and with it the quantity log $\{\Psi(Y, a)\,[G_\lambda^m(x)/G_\lambda^0(x)]\}$, which is the horizontal distance between the log $G_\lambda^m(x)/G_\lambda^0(x)$ curve for the particular $x = \log \tau_{\lambda_0}$ and the log $\Psi(Y, a)$ curve for the damping, a. We have used Traving's estimate of the damping constant, since we felt that his values were not likely to be improved substantially until new data on the Stark broadening were available. These distances $|\log \Psi(Y, a)G_\lambda^m(x)/G_\lambda^0(x)|$ are now subtracted graphically from the local value of the curve log $Z(x)(1 - 10^{-\theta x_\lambda})$ in order to construct the function

$$\log Z\,(x)\,(1 - 10^{-\theta x_\lambda})\,\Psi\,(Y, a)\,\frac{G_\lambda^m\,(x)}{G_\lambda^0\,(x)}.$$

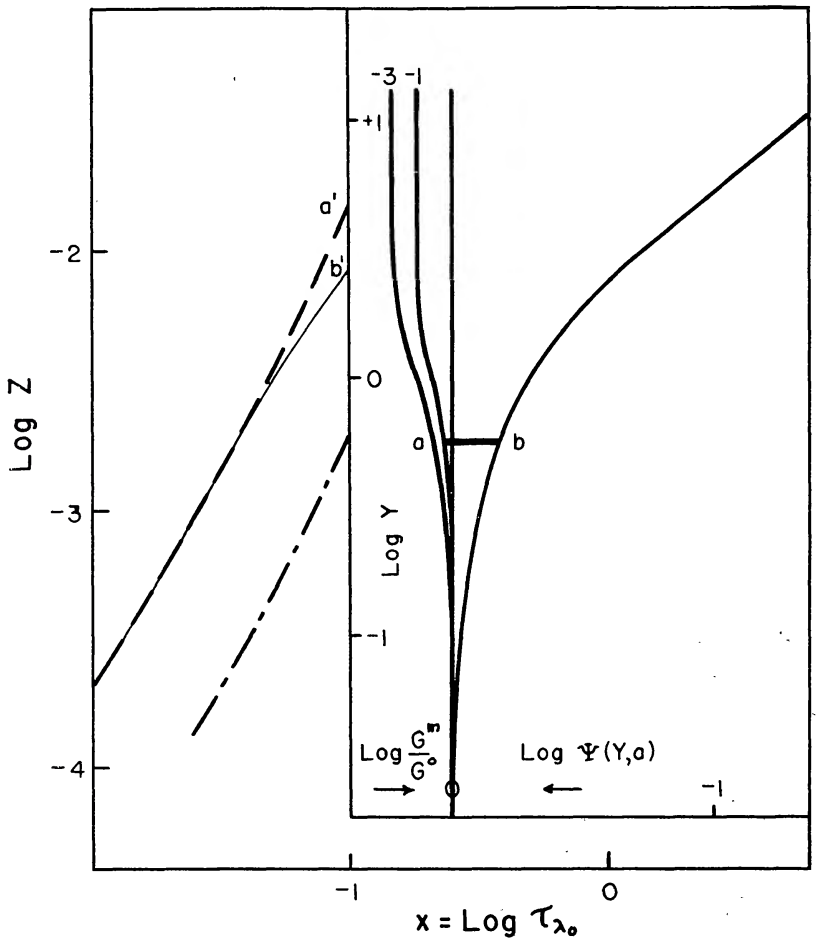

FIG. 5.—Graphical method in the calculation of an exact curve of growth. The graph of the saturation function, log $\Psi(Y, a)$ and the saturation weight, log $G_\lambda^m(x)/G_\lambda^0(x)$ (cf. Fig. 1) is superposed on the graph of log $Z(x)$, log $Z(x)(1 - 10^{-\theta x_\lambda})$, etc., with the Ψ-axis parallel to the $x = \log \tau_{\lambda_0}$ axis. In the example shown (Si IV), the log $Y = 0$ position coincides with log $Z(x) = -2.49$ for log $M = -2.50$. The figure depicts the calculation of a point on the

$$\log Z(x)(1 - 10^{-\theta x_\lambda})\,\frac{G_\lambda^m(x)}{G_\lambda^0(x)}\,\Psi(Y, a)$$

curve (*solid lines*) at a point $x = -1.0$. The quantity to be subtracted from the log $Z(x)(1 - 10^{-\theta x_\lambda})$ curve (*dashed line*) is denoted by $a - b = a' - b'$. The dot-dash curve gives the function

$$\log \sqrt{\theta} \int_{-\infty}^{x} Z(x)(1 - 10^{-\theta x_\lambda})\,dx,$$

which is needed to fix the position log $Y = 0$ (see text).

We now read out the antilog of this function in steps of $\Delta x = 0.2$ with the aid of a logarithmic scale, multiply by $G^0_\lambda(x)$, and add up to obtain $\mathfrak{L}^*_\lambda$ according to equation (51), in the same way as described for L^*_λ on pages 13 and 14. As a result of these operations, we finally obtain the difference

$$\log L^*_\lambda - \log \mathfrak{L}^*_\lambda = \Delta ,$$

which is the distance of the actual curve of growth from the 45° line at a point where this line has the chosen ordinate $\log W_\lambda/\lambda$. For our example, $\log W_\lambda/\lambda = -4.45$, and Δ becomes 0.65. The same calculation is carried out for two or three values of $\log M$ in order to get the theoretical curve of growth. The difference Δ depends highly on the gradient of $\log Z(x)$, so that the curve of growth for the two stages of ionization of the same element may differ considerably, as we shall see in the actual curves of growth. In the case of a very steep gradient (i.e., where the greatest contribution to the absorption comes from the deep layers), the influence of the weight function, which in that region depends strongly on the wave length, also produces a wave-length dependence of the curve of growth. The result of the calculation is that the increase in the number of absorbing atoms with depth in the atmosphere determines how fast the saturation of the lines sets in with growing line strength. The physical picture is that the formation of a line depends on how rapidly the number of absorbing atoms increases with depth in the atmosphere and how rapidly the continuous absorption increases. If the continuum is primarily formed above the line, the line will be substantially weaker than one which is formed mostly in the upper layers.

Once having the theoretical curve of growth, we shift it horizontally so that it represents the points of the empirical curve of growth. Now the position of the 45° line gives the relation between the $\log W_\lambda/\lambda$ and $\log C$, which is, according to equation (53), the logarithm of the abundance of that element, $\log (N_i/N_H)$. If in some elements two or three stages of ionization are observed, the resulting abundance should be the same, assuming that the model atmosphere and the mechanism of line formation are correct. In the case of systematic disagreements for all those elements which are observed with sufficient accuracy in more than one ionization stage, we may conclude that the model has to be re-examined. A slight change in the intrinsic temperature and electron pressure may lead to a better representation of the observations. As we shall see, errors in the f-values or equivalent widths may cause considerable complications.

The Oscillator Strengths

The quantity $\tilde{f}$ was used by Unsöld (1941*b*) and is related to the conventional or Ladenburg f by the expression (see, e.g., Goldberg, Aller, and Müller, 1954)

$$\tilde{f}(aJ;\ a'J') = \bar{f}\,\frac{S}{\Sigma S}\,\frac{s}{\Sigma s}\,\frac{\bar{\lambda}}{\lambda} = \frac{2J'+1}{\Sigma g_i}\, f(aJ;\ a'J') , \tag{70}$$

where $\bar{f}$ is the mean oscillator strength for the whole transition array (Bates and Damgaard 1948), S is the strength of the multiplet, s is the strength of the line under consideration, the $a'J'$'s refer to the energy-level designation and J-value of the lower level, the aJ's the corresponding quantities for the upper level, and the Σg_i is taken over the statistical weights of all the levels in the reference term or in the whole configuration, as the circumstances warrant. In O II and Ne II refer the f's to the 3s, 3p, or 3d lower configurations; in other ions they are referred to the designated *reference terms*. The $\tilde{f}$ has the convenient property that

$$N_{J'} f(aJ;\ a'J') = N_c \tilde{f}(aJ;\ a'J') , \tag{71}$$

where $N_{J'}$ is the number of atoms in the lower level and N_c is the number in the whole

configuration or reference term. In practice, the slight wave-length variation in $\bar{\lambda}/\lambda$ may be neglected.

The f-values for the transitions observed have usually been calculated on the basis of LS coupling, which appears to be a good approximation for many light atoms. For some multiplets of O II, Ne II, S II, and A II, Garstang (1954) has obtained line strengths in intermediate coupling. We have used his line strengths whenever they were available. It is urgently desired that these calculations be extended to other transitions and to other ions.

The radial quantum integrals $\sigma(n'l'; nl)$ for high-level transitions in light atoms may be approximated by the methods of Bates and Damgaard (1949). In the ions of oxygen or neon we have calculated a mean σ^2 for the whole transition array rather than use a particular σ for each multiplet.

The Equivalent Widths

The fifth column in Table 5 gives the equivalent widths of the lines expressed in milliangstroms. These values are based on observations secured with the Mount Wilson and McDonald coudé spectrographs. The Mount Wilson observations were obtained with the 114-inch camera, which gives a dispersion of 2.8 A/mm. Earlier plates secured by Walter S. Adams, Paul Merrill, and R. F. Sanford and kindly made available to us were supplemented by data secured by one of us in 1955. We are deeply indebted to Director Bengt Strömgren and to Helmut Abt for a number of excellent plates secured with the new grating coudé spectrograph of the McDonald Observatory. Six plates covering the photographic region have been used in the compilation of observational data.

The equivalent widths obtained from the McDonald and Mount Wilson plates are generally in good agreement with one another, except that in the blue region $\sim \lambda\,4600$, the McDonald equivalent widths seem to be a bit larger. On the other hand, both sets of measures often disagree markedly with the ones published by Unsöld, particularly with those based on Cassegrain spectrograph plates. The W_λ measurements with the lower-dispersion spectrographs tend to be systematically larger than those found with the high-dispersion grating plates. The differences appear to be larger for the weaker lines. Pending further investigation of this matter, we have used only the Mount Wilson and newer McDonald observations in our theoretical analyses. Before further discussions of the spectrum of this star are undertaken, a thorough system of accurate equivalent widths should be established.

Discussion of the Curves of Growth

The abscissa of the curve of growth, log C, has been computed as described on the preceding pages, with $\theta_0 = 0.18$. The last column of Table 5 gives the blend with another element (if any). Blended lines are usually to be rejected in curve-of-growth analyses unless it can be shown that one of the component ions contributes a negligible amount. Many lines, particularly of O II, fall on the wings of the strong Balmer lines. Hence they are weakened by the increased hydrogen absorption, which acts just as though the continuous absorption coefficient were increased. If we are entitled to assume that the lines of hydrogen and those of the ion under consideration are formed in the same optical layers, we may make a rough correction to log C (cf., e.g., Unsöld 1938). We have made this correction for a number of lines, and, although we can assert that the correction to log C is in the right direction, we cannot be sure that it is quantitatively reliable.

Carbon, nitrogen, oxygen, and silicon are observed in two stages of ionization; hence they provide a particularly valuable check on the model atmosphere. Preliminary results for silicon and for the profile of Hγ (Elste *et al.* 1956) suggested that our revised Traving model was satisfactory for the abundance analysis. Hence we used it to carry out calculations for the other elements, which we shall discuss in turn.

TABLE 5

DATA FOR OBSERVED LINES OF VARIOUS ELEMENTS IN τ SCORPII

MULT.	TRANSITION OR REFERENCE TERM	λ	log $\tilde{f}$	W_λ	log W_λ/λ	log C	BLENDS
			Carbon				
C II:							
(33)	$3d^4F-4f^4G$	3876.05, 76.19	−0.43	40	−4.99	+0.02	
		76.41, 76.67	−0.46	35	−5.05	−0.01	
(6)	$3d^2D-4f^2F$	4267.27	−0.26	50	−4.93	−0.36	
		67.02	−0.42	40	−5.03	−0.54	
(4)	3^2P-4^2S	3920.68	−1.04	27	−5.16	−1.00	
C III:							
(24)	4^1D-5^1F	4056.06	−0.29	34	−5.08	−0.97	
(16)	4^3F-5^3G	4070.30	−0.26	51	−4.90	− .29	
		4068.97	−0.37	54	−4.88	− .40	
		4067.87	−0.49	49	−4.92	− .52	
(18)	4^1F-5^1G	4187.05	+0.13	66	−4.80	− .39	
(1)	$3^3S-3^3P^0$	4647.40	−0.38	177	−4.42	+ .32	
		4650.16	−0.60	143	−4.51	+ .10	
		4651.35	−1.07	110	−4.63	−0.37	
			Nitrogen				
N II:							
(12)	$3s(^1P+^3P)$	3995.00	−0.88	75	−4.72	−0.50	
(5)	$g=12$	4630.54	−1.00	63	−4.87	−0.71	
		4643.09	−1.48	36	−5.11	−1.19	
		4621.39	−1.57	21	−5.34	−1.28	
		4601.48	−1.48	30	−5.18	−1.18	
		4607.15	−1.57	39	−5.07	−1.27	
(15)	$3p^1P$; $g=3$	4447.02	−0.21	48	−4.97	−0.86	
(39)	$3d(^3P+^3D+^3P)$, $g=45$	4041.32	−0.76	50	−4.90	−0.68	
		4043.54	−0.90	37	−5.04	−0.79	
		4035.09	−1.02	37	−5.04	−0.91	O II?
(38)		4082.28		17:	−5.37		
(48)		4241.79	−0.93	46	−4.96	−0.88	
		4237.05, 4236.93	−0.87	45	−4.97	−0.82	
(55)		4432.74	−1.05	27	−5.22	−1.04	
		4433.48	−1.68	12	−5.57	−1.70	
		4442.00	−1.33			−1.35	
(42)	$3p^1P$; $g=3$	4176.16	−0.57	25	−5.22	−1.73	
(59)		4530.40	−0.40	31	−5.17	−1.61	
(30)	$3p(^1S, ^1P, ^1D)+(^3S, ^3P, ^3D)$	3838.39	−1.80	27	−5.15	−1.41	S III H 21 per cent
		3855.08	−2.37	10	−5.58	−1.99	
(33)	$g=36$	4227.75	−1.75	26	−5.21	−1.40	

TABLE 5—*Continued*

Mult.	Transition or Reference Term	λ	log $\tilde{f}$	W_λ	log W_λ/λ	log C	Blends
			Nitrogen—*Continued*				
N III:							
(2)	$3p^2P$, $g=6$	4634.16	−0.85	73	−4.80	−0.36	
		4640.64	−0.59	87	−4.72	−0.10	
		4641.90	−1.55	123	−4.57	−1.06	O II
(16)	$4d^2D$, $g=10$	4003.64	−0.38	36	−5.04	−0.89	
		3998.69	−0.54	31	−5.11	−1.05	S II?
(3)	$2s^2p3s$ ($^2P+^4P$)	4514.89	−1.04	55	−4.92	−0.85	
		4510.92	−1.17	49	−4.96	−1.02	
(6)	$g=18$	4200.02	−1.16	34	−5.09	−1.11	
		4195.70	−1.44	38	−5.04	−1.39	
			Oxygen				
O II:							
(1)	3s − 3p, $^4P-^4D^0$	4676.23	−1.70	82	−4.76	−1.02	
		4661.64	−1.57	84	−4.74	−0.88	
		4641.81	−1.25	123	−4.58	−0.56	N III
		4638.85	−1.64	82	−4.75	−0.95	
		4673.75	−2.40	55	−4.93	−1.73	C III
		4650.84	−1.66	95	−4.69	−0.97	
		4649.14	−0.99	139	−4.52	−0.29	
(2)	$^4P-^4P^0$	4317.14	−1.73	67	−4.81	−0.99	
		4319.63	−1.70	72	−4.78	−0.96	
		4325.77	−2.42	59	−4.87	−1.68	C III 1 per cent
		4345.56	−1.67	59	−4.87	−0.93	11 per cent Hγ
		4349.43	−1.26	96	−4.66	−0.52	5 per cent Hγ
		4366.90	−1.61	77	−4.75	−0.88	
(6)	$^2P-^2P^0$	3945.05	−2.13	39	−5.00	−1.42	S II
		3954.37	−1.76	65	−4.78	−1.06	1 per cent
		3973.26	−1.35	51	−4.89	−0.65	20 per cent H
		3982.72	−2.08	38	−5.02	−1.38	3 per cent H
(5)	$^2P-^2D^0$	4414.91	−1.11	104	−4.63	−0.48	
		4416.98	−1.36	84	−4.72	−0.73	
		4452.38	−2.11	40	−5.05	−1.48	
(10)	3p − 3d, $\overline{^4D^0}-\overline{^4F}$	4075.87	−1.16	98	−4.62	−0.40	
		4072.16	−1.31	88	−4.66	−0.54	
		4069.90	−1.50	70	−4.76	−0.74	
		4069.64	−1.69	70	−4.76	−0.93	
		4092.94	−2.17	35	−5.06	−1.41	4 per cent H
		4085.12	−2.03	42	−4.99	−1.27	3 per cent H
		4078.86	−2.14	46	−4.95	−1.38	

TABLE 5—*Continued*

Mult.	Transition or Reference Term	λ	log $\tilde{f}$	W_λ	log W_λ/λ	log C	Blends
		Oxygen—*Continued*					
O II:							
		4119.22	−1.41	85	−4.68	−0.70	1 per cent
		4104.74	−2.01	13	−5.50	−1.30	20 per cent H
		4097.26	−2.65	91B	−4.66	−1.93	16 per cent H, N III
(20)	$^4P^0-{}^4D$	4120.28	−1.80	.....	.....	−1.09	8 per cent H
		4120.55	−2.38	29	−5.15	−1.67	O II
		4105.00	−1.90	30	−5.14	−1.19	20 per cent H
		4110.80	−2.27	32	−5.11	−1.56	6 per cent H
		4169.22	−2.35	44	−5.00	−1.65	.....
		4121.48	−2.80	23	−5.25	−2.09	6 per cent H
(19)	$^4P^0-{}^4P$	4156.54	−2.68	55B	−4.88	−1.97	C III
		4153.30	−1.81	74	−4.75	−1.10	S II
		3882.20	−1.90	45	−4.93	−1.11	6 per cent H
(12)	$^4D^0-{}^4D$	3864.45	−2.29	22	−5.25	−1.50	.....
(21)	$^4P^0-{}^2F$	4112.01	−2.66	31	−5.12	−1.95	5 per cent H
(36)	$^2\bar{F}^0-{}^2\bar{G}$	4185.46	−1.27	59	−4.85	−1.07	.....
		4395.95	−1.99	44	−5.00	−1.42	.....
(26)	$^2D^0-{}^3D$	4369.28	−2.22	25	−5.24	−1.63	.....
		4448.21	−1.75	35	−5.10	−1.60	.....
(35)	$^2F^0-{}^2F$	4443.05	−1.88	23	−5.28	−1.73	.....
(61)	$^2\bar{P}^0-{}^2\bar{S}$	4319.93	−2.34	72	−4.78	−1.26	O II
		4327.48	−1.67	25	−5.24	−1.52	1 per cent
(41)	$^2\bar{D}^0-{}^2\bar{D}$	4331.89	−1.83	15	−5.46	−1.66	4 per cent
(11)	$^4D^0-{}^4P$	3907.45	−3.35	18	−5.34	−2.54	.....
(25)	$^2D^0-{}^2F$	4705.36	−1.27	80	−4.77	−0.74	.....
(40)	$^2\bar{D}^0-{}^2\bar{F}$	4699.21	−1.46	89	−4.72	−1.38	O II
(13)	$^2D^0-{}^2F$	3857.18	−3.12	23	−5.22	−2.33	.....
	3d−4f	4089.30	−1.28	66	−4.81	−0.87	3 per cent
(48)	$^4F-{}^4G^0$	4095.63	−1.52	19	−5.33	−1.11	12 per cent
		4087.16	−1.64	44	−4.97	−1.23	2 per cent
		4275.52	−1.41	51	−4.92	−1.06	.....
(67)	$^4D-{}^4F^0$	4276.71	−1.57	34	−5.10	−1.22	O II
		4277.40	−1.96	26	−5.21	−1.61	.....
(54)	$^4P-{}^4D^0$	4303.82	−1.53	61	−4.85	−1.19	.....
(101)	$^2\bar{G}-{}^2H^0$	4253.74	−1.27	26	−5.21	−1.40	.....
		4253.98	−1.36	26	−5.21	−1.49	.....
(93)	$^2D-{}^2F^0$	4609.42	−1.50	41	−5.05	−1.25	.....
		4602.11	−1.66	34	−5.13	−1.41	.....
(86)	$^2P-{}^2D^0$	4491.25	−1.65	28	−5.21	−1.36	.....
(102)	$^2\bar{D}-{}^2\bar{F}^0$	4378.41	−1.71	23	−5.28	−1.45	.....
		4378.01	−1.87	21	−5.32	−1.61	.....
(64)	$^4D-{}^4D^0$	4308.96	−3.16	17	−5.40	−2.83	.....

TABLE 5—*Continued*

Mult.	Transition or Reference Term	λ	log $\tilde{f}$	W_λ	log W_λ/λ	log C	Blends
			Oxygen—*Continued*				
O III:							
(2)	$^3P+{}^1P$, $g=12$	3759.87	−0.88	76	−4.69	−0.29	.....
		3757.21	−1.50	31	−5.08	−0.91	3 per cent
		3791.26	−1.63	45	−4.92	−1.04	6 per cent Si III
(14)	$^3P+{}^1P$, $g=12$	3707.24	−1.01	25:	−5.17	−1.04	3 per cent
		3715.08	−1.74	17:	−5.34	−1.77	1.5 per cent
			Neon				
Ne II:							
(7)	$3s-3p$, $^2P-{}^2P^0$	3323.75	−1.55	30	−5.04	−0.91	.....
(5)	$^2P-{}^2D^0$	3643.89	−2.06	30	−5.08	−1.46	.....
		3713.09	−1.25	65:	−4.76	−0.65	2 per cent H
		3727.08	−1.55	49:	−4.88	−0.94	.....
(1)	$^4P-{}^4P^0$	3664.09	−1.80	50	−4.86	−1.09	.....
		3694.22	−1.36	68	−4.73	−0.65	.....
		3709.64	−1.80	40	−4.97	−1.09	.....
(2)	$^4P-{}^4D^0$	3327.16	−1.74	40	−4.92	−0.99	.....
		3334.87	−1.13	54	−4.79	−0.38	.....
		3355.05	−1.37	55	−4.78	−0.61	.....
		3360.63	−1.75	34	−5.00	−0.99	.....
		3344.43	−1.80	31	−5.03	−1.04	.....
(10)	$3s^2D-3p^2P$	3345.49	−1.48	40	−4.92	−1.33	.....
		3345.88	−2.44				
(9)	$3s^2D-3p^2F^0$	3568.53	−1.13	44	−4.91	−1.01	.....
		3574.64	−1.29	28	−5.10	−1.18	.....
		3574.23	−2.40	8	−5.65	−2.29	.....
(12)	$3p^4D^0-3d^4D$	3329.20	−1.65	16:	−5.32	−1.31	.....
(20)	$3p^2D^0-3d^2F$	3417.71	−1.27	20:	−5.23	−0.99	.....
(34)	$3p^4S^0-3d^4P$	3542.90	−1.55	21	−5.23	−1.33	.....
			Aluminum				
Al III:							
(8)	4^2F-5^2G, $g=14$	4480.0	0.00	26	−5.24	+0.64	.....
		.....	.....	.....	.....	.....	.....
(3)	$4^2P^0-4^2D$, $g=6$	4529.18	− .11	32	−5.15	+ .68	.....
		4512.54	−0.37	25	−5.26	+0.42	.....
			Magnesium				
Mg II:							
(4)	$3^2D-4^2F^0$	4481.33	.....	.....	.....	.....	.....
	$g=10$	4481.13	0.00	105	−4.63	+0.18	.....

Carbon.—C II is represented by three multiplets; the λ 3876 lines seem to be systematically too weak as compared with 3920 and 4267. We suspect that the *f*-values for the $^4F - {}^4G$ multiplet may be much smaller than indicated by theory, since the same discordance is found in other stars under investigation. The C III lines, a number of which are fairly strong, delineate a well-defined curve of growth.

The empirical curves for C II and C III do not fit the theoretical curves. That is, if the empirical curve for C II is fitted to the theoretical curve for the same ion, the theoretical curve for C III will fall below the empirical C III curve. This discordance would indicate that some revision of the model atmosphere was necessary.

Nitrogen.—The N II lines define a reasonably precise curve of growth, although λ 4176 and λ 4530 seem to be too strong for the stated *f*-values. The N III lines likewise define an empirical curve with relatively small scatter. Our measured intensities for the N III lines are all appreciably smaller than Unsöld's values, the discrepancy being considerably greater than for N II.

As with carbon, if the theoretical and empirical curves of the singly ionized element are fitted together, the empirical curve for the doubly ionized atom lies above the theoretical curve. Whatever correction is required for carbon, a correction in the same direction will be required for nitrogen.

Oxygen.—Extensive data are available for O II, so that it is possible to construct separate curves of growth for the 3s–3p, 3p–3d, and 3d–4f transition arrays. The 3s–3p-curve is the best defined, partly because line strengths for intermediate coupling are available and partly because blending with hydrogen lines does not have to be considered. The scatter is larger for the weaker lines, not only because the line intensities are less accurate but also because the errors in the *f*-values are likely to be greater. No corrections for deviations from LS coupling are available for the lines of the 3d–4f transition array.

The O III lines present a particularly interesting problem. All the observed lines are influenced to some extent by the overlapping wings of the Balmer lines. Of the three strongest lines λλ 3759.9, 3757.3, and 3791.4, the first is least affected by the blending, whereas the last falls in a wing of a hydrogen line and is also blended with Si III. The 3707 and 3715 lines are very weak. We have roughly calculated the blending corrections by the afore-mentioned Unsöld procedure, but we must emphasize that this correction amounts to an underestimate, since the O III lines are predominantly formed *below* the hydrogen lines. These O III lines would be greatly strengthened if we could but see them freed from the strong absorption of the Balmer lines. We should calculate weighting functions for each of these lines, taking into account the continuous plus the line absorption in hydrogen. Such a laborious calculation is not merited until much better *f*-value and line-intensity data are available. Accordingly, we have not used the O III data in our differential correction to the model atmosphere.

Neon.—This element is represented by a number of strong ultraviolet lines of Ne II. Our *f*-values differ from those of Traving because we have used Garstang's line strengths for intermediate coupling and because we have used mean values for σ for the 3s–3p and 3p–3d configurations.

Aluminum.—Only three lines, λλ 4480, 4512, 4529, of Al III are available in this star.

Magnesium.—This element is represented only by the close doublet λ 4481 in τ Scorpii.

The discrepancies in the curves of growth for carbon and for nitrogen show that another small adjustment in the temperature (and perhaps also in the electron pressure) is necessary. At the same time, the adopted atmosphere represented the Si III and Si IV lines fairly well. We shall show in Section VI that a slight adjustment in the temperature scale will improve the agreement between theory and observation for carbon and nitrogen without at the same time destroying the fit for silicon. It appears impossible, how-

ever, to secure an adjustment of the atmospheric parameters that will simultaneously fit all elements equally well!

After the adjustments in θ and log P_e have been made, it is possible to derive corrections to the abundances of all observed elements (see Sec. VII).

VI. A DIFFERENTIAL CORRECTION TO THE MODEL ATMOSPHERE

If the model atmosphere we have adopted does not represent the observations of both stages of ionization of an element, either we may calculate log C for other model atmospheres and interpolate, or, if suitable model atmospheres are not available, we must undertake a differential correction. The abscissa of the curve of growth changes differently for the three important ionization stages.

Consider the change in abscissa for a change in temperature in the atmosphere cor-

TABLE 6

OPTICAL DEPTH OF THE FORMATION OF LINES IN τ SCORPII

	$\langle \log \tau_{\lambda_0} \rangle$	$\langle \theta \rangle$		$\langle \log \tau_{\lambda_0} \rangle$	$\langle \theta \rangle$
Si III.....	−1.1	0.189	C II.....	−1.2	0.195
Si IV.....	−0.3	.158	C III.....	−0.4	.162
N II.....	−0.9	.180	O II.....	−1.0	.185
N III.....	−0.15	0.152	O III.....	−0.4	0.162

responding to $\Delta\theta$ and for a change in electron pressure $\Delta \log P_e$. Then (compare Traving 1955, eq. [35]), or by differentiation of equation (66), $\Delta \log C$ will be given by

$$\Delta \log C = (\chi_{r-1} - \chi_{r-1,\,s})\,\Delta\theta + \tfrac{5}{2}\,\mathrm{Mod}\,\frac{\Delta\theta}{\theta} + \Delta \log P_e - \Delta \log U_r - \Delta \log (\kappa^\lambda + \sigma) + \Delta \log G_\lambda^*,$$

$$\Delta \log C = -\chi_{r,\,s}\Delta\theta - \Delta \log U_r - \Delta \log (\kappa^\lambda + \sigma) + \Delta \log G_\lambda^*, \tag{72}$$

$$\Delta \log C = -(\chi_r + \chi_{r+1,\,s})\,\Delta\theta - \tfrac{5}{2}\,\mathrm{Mod}\,\frac{\Delta\theta}{\theta} - \Delta \log P_e - \Delta \log U_r - \Delta \log (\kappa^\lambda + \sigma) + \Delta \log G_\lambda^*,$$

where

$$\Delta \log U_r = \frac{\partial \log U_r}{\partial \theta}\,\Delta\theta + \frac{\partial \log U_r}{\partial \log P_e}\,\Delta \log P_e, \tag{73}$$

$$\Delta \log (\kappa^\lambda + \sigma) = \frac{\partial \log (\kappa^\lambda + \sigma)}{\partial \theta}\,\Delta\theta + \frac{\partial \log (\kappa^\lambda + \sigma)}{\partial \log P_e}\,\Delta \log P_e. \tag{74}$$

For small corrections in temperatures and electron pressures, the change in the weight function will amount to a second-order effect, which can be neglected (cf. also Traving 1955).

We have to evaluate the differential coefficients at the mean depth $\langle \log \tau_{\lambda_0} \rangle$ at which the line is formed. This depends on the stage of ionization, the lines of the higher stage of ionization being formed naturally in the deeper layers (see Table 6). Thus the lines of

C II, N II, O II, and Si III tend to be formed around a depth of 0.1, whereas the lines of the next higher stage of ionization are primarily formed in substantially deeper layers.

The differential coefficients $\partial \log (\kappa^{\lambda} + \sigma)/\partial\theta$ and $\partial \log (\kappa^{\lambda} + \sigma)/\partial \log P_e$ are to be found easily from a numerical differential of the Kyoto continuous absorption-coefficient tables (Ueno *et al.* 1954). The partial derivatives of U_r with respect to θ and P_e may be discussed as follows:

Let us write:

$$U_r = u_1 + u_2 + u_3 = u_{r-1} 10^{+\chi_{r-1}\theta - \zeta(x)} + u_r + u_{r+1} 10^{-\chi_{r+1}\theta + \zeta(x)}, \tag{75}$$

where

$$\zeta(x) = 9.080 - \tfrac{5}{2} \log \theta - \log P_e. \tag{76}$$

We can write

$$\frac{\partial \log U_r}{\partial \theta} = \frac{\text{Mod}}{U_r} \frac{\partial U_r}{\partial \theta} = \frac{\text{Mod}}{U_r} \left(\frac{\partial u_1}{\partial \theta} + \frac{\partial u_2}{\partial \theta} + \frac{\partial u_3}{\partial \theta} \right), \tag{77}$$

where now

$$\begin{aligned} \frac{\partial u_1}{\partial \theta} &= \frac{\partial u_{r-1}}{\partial \theta} 10^{+\chi_{r-1}\theta - \zeta(x)} + u_{r-1} \frac{\partial}{\partial \theta} e^{1/\text{Mod}\,[\chi_{r-1}\theta - \zeta(x)]} \\ &= \frac{\partial u_{r-1}}{\partial \theta} \frac{1}{u_{r-1}} u_{r-1} 10^{\chi_{r-1}\theta - \zeta(x)} + u_{r-1} 10^{\chi_{r-1}\theta - \zeta(x)} \frac{1}{\text{Mod}} \frac{\partial}{\partial \theta} [\chi_{r-1}\theta - \zeta(x)] \\ &= \left\{ \frac{1}{\text{Mod}} \frac{\partial \log u_{r-1}}{\partial \theta} + \frac{1}{\text{Mod}} \left[\chi_{r-1} - \frac{\partial}{\partial \theta} \zeta(x) \right] \right\} u_{r-1} 10^{+\chi_{r-1}\theta - \zeta(x)}. \end{aligned} \tag{78}$$

Since

$$-\frac{\partial}{\partial \theta} \zeta(x) = +\tfrac{5}{2} \text{Mod} \frac{\partial \theta}{\theta \partial \theta} = \frac{1.086}{\theta}, \tag{79}$$

we have

$$\frac{\partial u_1}{\partial \theta} = \text{Mod}^{-1} u_1 \left(\frac{\partial \log u_{r-1}}{\partial \theta} + \chi_{r-1} + \frac{1.086}{\theta} \right) \tag{80}$$

and, similarly,

$$\frac{\partial u_3}{\partial \theta} = \text{Mod}^{-1} u_3 \left(\frac{\partial \log u_{r+1}}{\partial \theta} - \chi_r - \frac{1.086}{\theta} \right). \tag{81}$$

Hence

$$\begin{aligned} \frac{\partial \log U_r}{\partial \theta} = \frac{u_1}{U_r} \left(\frac{\partial \log u_{r-1}}{\partial \theta} + \chi_{r-1} + \frac{1.086}{\theta} \right) + \frac{\text{Mod}}{U_r} \frac{\partial u_r}{\partial \theta} \\ + \frac{u_3}{U_r} \left(\frac{\partial \log u_{r+1}}{\partial \theta} - \chi_r - \frac{1.086}{\theta} \right); \end{aligned} \tag{82}$$

and likewise we find, by partial differentiation with respect to $\log P_e$,

$$\frac{\partial \log U_r}{\partial \log P_e} = \frac{u_1 - u_3}{U_r}. \tag{83}$$

Table 7 displays $\partial \log U_r/\partial\theta$ and $\partial \log U_r/\partial \log P_e$ as calculated for $\theta = 0.22$, 0.18, and 0.14, corresponding to the top of the atmosphere, a kind of average depth where the lines are formed, and a deeper layer. Notice that these partial derivatives depend strongly on both the optical depth and the element. Hence, by differentially correcting a model atmosphere by an amount $\Delta\theta$ or $\Delta \log P_e$, the relative abundances will not all be changed by the same amount.

VII. THE ADOPTED COMPOSITION

An application of the differential correction shows that no unique change in $\Delta\theta$ and $\Delta \log P_e$ can represent equally well the curves of growth for all elements. Silicon required the smallest change, and nitrogen the largest. For reasons indicated in Section V, we did not use the data for oxygen, although, when a final value was selected for $\Delta\theta$, the oxygen data appeared to be consistent with this choice.

After a few trials we found that the best over-all representation of the data could be found if we selected a $\Delta\theta = -0.01$ and $\Delta \log P_e = 0$. The evidence from the hydrogen lines indicated that the adopted electron-pressure distribution must be nearly correct; we could have gone to a slightly lower electron pressure, which would have required a slightly smaller change in $\Delta\theta$.

The final curves of growth are shown in Figures 6, 7, and 8. The abscissae, log C, have to be recalculated for the new value of θ_0, i.e., 0.17. The discrepancy between theory and

TABLE 7

DEPENDENCE OF DIFFERENTIAL COEFFICIENTS OF THE FUNCTION U_τ ON θ AND LOG P_e FOR DIFFERENT ELEMENTS

θ	$\partial \log U_\tau/\partial\theta$				$\partial \log U_\tau/\partial \log P_e$			
	Si	O	N	C	Si	O	N	C
0.22.....	+ 0.41	+ 2.9	− 0.16	− 1.68	+0.025	+0.086	+0.014	−0.0129
.18.....	−10.6	− 0.31	− 2.8	−13.6	− .195	+ .012	− .037	− .202
0.14.....	−45.0	−18.4	−35.3	−63	−0.847	−0.272	−0.593	−0.864

observation is now of the same order as the observational errors themselves, although we feel that an actual discrepancy may very well exist. Part of the discrepancy may be due to the uncertainties in the f-values, but some of it may arise from the model atmosphere itself. We have assumed plane-parallel stratified layers in radiative equilibrium and no distortion of the star due to rotation. If the star is actually rotating rapidly and we are looking down on its pole, the T-log P_e-τ_0 relationship would vary from one part of the stellar disk to another, and we would have to consider the contributions from zones of different effective surface gravity. Further speculation on this point would appear inappropriate at present.

The finally adopted abundances of the heavier elements, expressed as log N_{element} N_{hydrogen}, are as follows:

Carbon.....	−4.3	Neon.....	−3.14
Nitrogen.....	−3.74	Magnesium.....	−3.7
Oxygen.....	−3.37	Aluminum.....	−5.6
Silicon.....	−4.37		

Our abundances are generally lower than those found by Traving, except for neon, where we find a somewhat higher abundance—indeed, neon would appear to be more abundant than oxygen. This result must be accepted with reserve until other stars have been examined. Further investigations of high-temperature stars, now in progress, may assist in this problem.

Since main-sequence B stars are formed relatively recently from the interstellar medium, which presumably has been enriched in helium and heavier elements in the five billion years since the sun was formed, we might anticipate the compositions of the sun and τ Scorpii to differ significantly. We would expect a much higher oxygen group

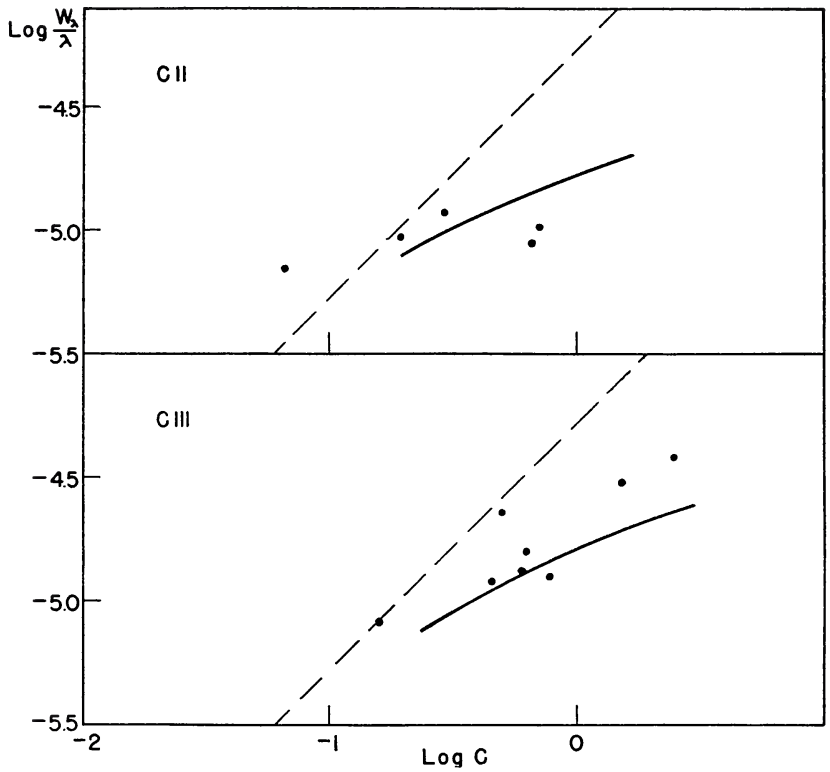

FIG. 6.—Curves of growth for carbon. Carbon is represented in τ Scorpii by C II and C III. The C II curve of growth is poorly defined. The straight line of inclination 45° corresponds to zero saturation. The solid curves are calculated by theory. Ordinates are log W_λ/λ; abscissae are log C in Figs. 6, 7, 8, 9, and 10.

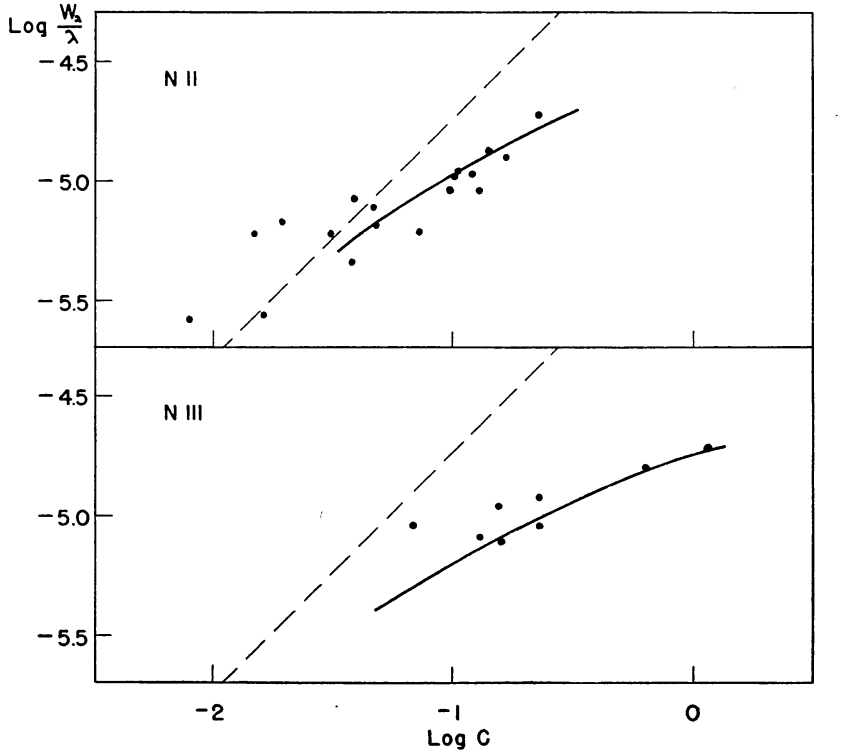

FIG. 7.—Curves of growth for nitrogen

to hydrogen ratio in τ Scorpii than in the sun. A comparison of our results with those of Goldberg *et al.* (1954) for the sun does not indicate that such a difference is clearly established. In fact, it would appear that no conclusions can be drawn until the accuracy of the abundance determinations can be improved. A study of additional B stars, now in progress, may be of some help.

Another possibility is that the enrichment of the interstellar medium proceeds at a much slower rate now than it did in the earlier history of the Galaxy when the sun was formed. A larger proportion of massive stars might have condensed out of the medium than is possible at present, with the consequence that heavy elements were formed at a much greater rate then than now. Possibly in a stellar system such as Messier 33 we now are witnessing circumstances more favorable to the formation of massive stars than exist in our own Galaxy.

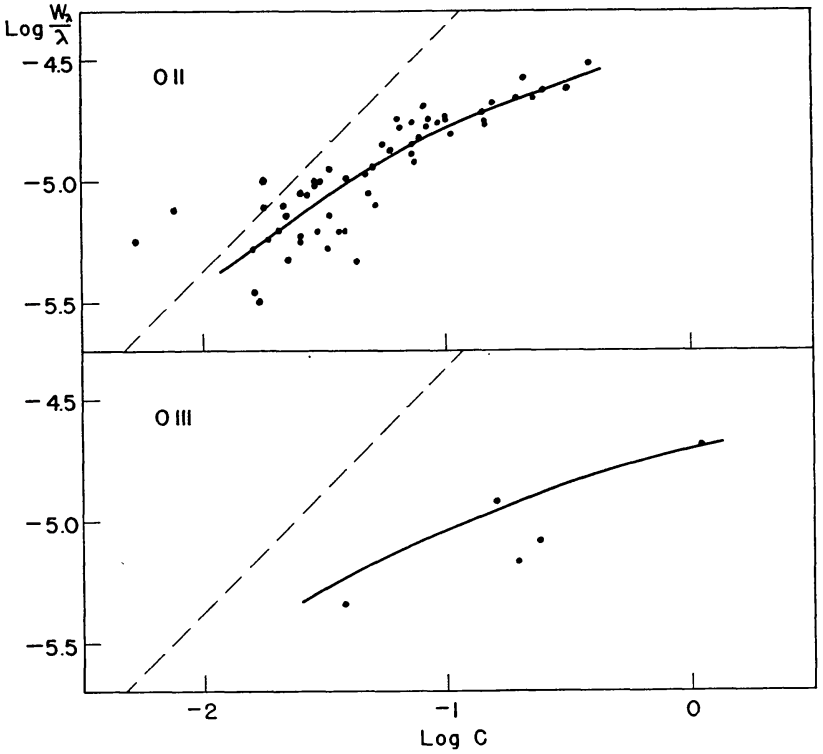

FIG. 8.—Curves of growth for oxygen. O II is represented by many lines of the 3s–3p, 3p–3d, and 3d–4f configurations. O III is represented by only a few lines, some of which are blended with the wings of hydrogen lines.

This program has been supported by a grant from the National Science Foundation. Thanks are due to Messrs. Merrill and Sanford and to the late Director Walter S. Adams of the Mount Wilson Observatory for their loan of spectroscopic material. We are particularly indebted to Director Bengt Strömgren and to Mr. Helmut Abt, of the Yerkes and McDonald Observatories, who obtained for us a number of excellent high-dispersion spectra of this star. Mr. G. Traving kindly supplied us with unpublished data on his model atmosphere. Finally, one of us, Jun Jugaku, would like to express his gratitude for a Fulbright Fellowship which made his work in this country possible.

REFERENCES

Aller, L. H. 1953, *The Atmospheres of the Sun and Stars* (New York: Ronald Press Co.), p. 267.
Barbier, D., and Chalonge, D. 1941, *Ann. d'ap.*, 4, 30.

Bates, D. R., and Damgaard, A. 1948, *Ap. J.*, **107**, 383.
———. 1949, *Phil. Trans. R. Soc. London, A*, **242**, 101.
Chalonge, D., and Divan, L. 1952, *Ann. d'ap.*, **15**, 235.
Chandrasekhar, S. 1950, *Radiative Transfer* (Oxford, England: Clarendon Press).
Claas, W. J. 1951, *Rech. Astr. Obs. Utrecht*, Vol. **12**, Part 1.
Elste, G. 1955, *Zs. f. Ap.*, **37**, 201.
Elste, G., Jugaku, J., and Aller, L. H. 1956, *Pub. A.S.P.*, **68**, 23.
Garstang, R. 1954, *M.N.*, **114**, 118.
Goldberg, L., Aller, L. H., and Müller, E. 1954, *Proc. Stellar Atmospheres Conference, Indiana University*, ed. M. Wrubel, p. 142.
Jugaku, J., and Elste, G. 1957, *Ap. J.*, in press.
Moore, C. 1949, *Atomic Energy Levels*, Vol. 1 (Bureau of Standards Circ., No. 467).
Neven, L., and Jager, C. de. 1954, *B.A.N.*, **12**, 103.
Pecker, J.-C. 1950, *Ann. d'ap.*, **13**, 319, 433.
——— 1951, *ibid.*, **14**, 383.
———. 1953, *Inst. Ap. Contr. Ser. A*, No. 132.
Traving, G. 1955, *Zs. f. Ap.*, **36**, 1.
Ueno, S., Saito, S., and Jugaku, J. 1954, *Contr. Kyoto Inst. Ap.*, No. 43.
Underhill, A. 1950, *Pub. Copenhagen Obs.*, No. 151.
Unsöld, A. 1938, *Physik der Sternatmosphären* (Berlin: Julius Springer).
———. 1941*a*, *Zs. f. Ap.*, **21**, 1.
———. 1941*b*, *ibid.*, **21**, 22.
———. 1942, *ibid.*, p. 229.
———. 1944, *ibid.*, **23**, 75.

APPENDIX I

TABLE A1

INTEGRAL FOR COMPUTATION OF WEIGHT FUNCTIONS

$x=\log \tau_{\lambda_0}$	$m=0$	$m=\frac{1}{2}$	$m=1$	$x=\log \tau_{\lambda_0}$	$m=0$	$m=\frac{1}{2}$	$m=1$
−3.0.....	0.991	0.664	0.499	−0.8.....	0.574	0.439	0.352
−2.8.....	.987	.663	.498	−0.6.....	.454	.357	.292
−2.6.....	.980	.661	.497	−0.4.....	.326	.265	.221
−2.4.....	.971	.658	.495	−0.2.....	.204	.170	.146
−2.2.....	.958	.652	.492	0.0.....	.1037	.0894	.0785
−2.0.....	.939	.645	.488	+0.2.....	.0393	.0348	.0314
−1.8.....	.913	.633	.481	+0.4.....	.00962	.00873	.00806
−1.6.....	.876	.616	.470	+0.6.....	.001238	.00115	.001081
−1.4.....	.827	.590	.455	+0.8.....	.000062	.000059	.000056
−1.2.....	.761	.554	.431	+1.0.....	0.000001	0.000001	0.000001
−1.0.....	0.677	0.504	0.398				

$$\frac{1}{\Delta x}\int_{x}^{x+\Delta x} E_{m+2}(x)\,dx.$$

APPENDIX II

Nomographical Method for Integrating a Function Given on a Logarithmic Scale

Günther H. E. Elste

In astrophysics it is occasionally necessary to have the integral of a function as a function of the upper limit. Many times, the function covers several powers of 10, and it is easier to compute and plot the function on a logarithmic scale than on a linear scale. Further, the accuracy desired in these cases is not higher than a few per cent. So the conditions for an application of nomographical methods are fulfilled.

On a graph there may be given $\log f(x)$. We want

$$\log \int_{-\infty}^{x} f(x)\, dx . \tag{A1}$$

Usually for the range from $-\infty$ to a certain x_0 and, further, for certain suitable steps Δx beyond x_0, where $f(x)$ gives the largest contribution to the integral, the curve $\log f(x)$ may be approximated by straight lines.

Using the straight-line approximation, we obtain

$$\log f(x) = \log f(x_n) + b\,(x - x_n) \tag{A2}$$

or

$$f(x) = f(x_n)\, 10^{b(x-x_n)} . \tag{A2a}$$

We have, for the integral,

$$\int_{x_1}^{x_2} f(x)\, dx = f(x_n) \int_{x_1}^{x_2} e^{b/\mathrm{Mod}\,(x-x_n)}\, dx = f(x_n) \frac{\mathrm{Mod}}{b} \left[e^{b/\mathrm{Mod}\,(x-x_n)} \right]_{x_1}^{x_2}, \tag{A3}$$

which gives, for a single integral step,

$$\int_{x_n}^{x_n+\Delta x} f(x)\, dx = f(x_n) \frac{\mathrm{Mod}}{b} (10^{b\,\Delta x} - 1) , \tag{A3a}$$

and, for the integral used at the beginning of the integration,

$$\int_{-\infty}^{x_0} f(x)\, dx = f(x_0) \frac{\mathrm{Mod}}{b} . \tag{A3b}$$

If we take the logarithms of equations (A3*a*) and (A3*b*), we obtain

$$\log \int_{x_n}^{x_n+\Delta x} f(x)\, dx = \log f(x_n) + \log \left[\frac{\mathrm{Mod}}{b} (10^{b\,\Delta x} - 1) \right] \tag{A4a}$$

and

$$\log \int_{-\infty}^{x_0} f(x)\, dx = \log f(x_0) + \log \left(\frac{\mathrm{Mod}}{b} \right) . \tag{A4b}$$

This means that the quantity to add to the logarithm of the function in order to get the integral is dependent on the slope of $\log f(x)$ only. Therefore, for each slope b of the approximation line, we must add another value to the logarithm of the function to be integrated. Or, if we draw the straight lines of approximation with different slopes b with respect to the value of the integral over one step as reference point, each line has a different position.

In order to develop the formula for the envelope of all the straight lines, we subtract equation (A4*a*) for the integral over one step from equation (A2) for the straight lines. So we obtain

$$y \equiv \log f(x) - \log \int_{x_n}^{x_n + \Delta x} f(x)\, dx = -\log \left[\frac{\text{Mod}}{b} (10^{b\,\Delta x} - 1) \right] + b\,(x - x_n)\,; \quad \text{(A5)}$$

and, if $b \to 0$, there will be

$$y_0 = -\log \Delta x\,. \quad \text{(A6)}$$

In the equation for the difference

$$y - y_0 = +\log \left[\frac{\text{Mod}}{b\Delta x} (e^{b\,\Delta x/\text{Mod}} - 1) \right]^{-1} + b\,(x - x_n)\,, \quad \text{(A7)}$$

we call the parameter

$$\frac{b\Delta x}{\text{Mod}} = p \quad \text{(A8)}$$

and introduce natural logarithms. If we set

$$\frac{y - y_0}{\text{Mod}} = \eta \qquad \text{and} \qquad \frac{x - x_n}{\Delta x} = \xi\,, \quad \text{(A9)}$$

we obtain

$$\eta = \ln \left(\frac{p}{e^p - 1} \right) + p\,\xi\,. \quad \text{(A10)}$$

We write this equation for the straight lines (A10) in the form $F(\xi, \eta, p) = 0$; then the envelope is given by equation (A10) and $\partial F(\xi, \eta, p)/\partial p = 0$, i.e.,

$$0 = \frac{(e^p - 1)(e^p - 1 - p\,e^p)}{p\,(e^p - 1)^2} + \xi \quad \text{(A11)}$$

or

$$\xi = \frac{1}{p} \left(\frac{p}{1 - e^{-p}} - 1 \right). \quad \text{(A12)}$$

Now we put ξ from equation (A12) into the equation (A10) and obtain

$$\eta = -p - 1 + \ln \left(\frac{p}{1 - e^{-p}} \right) + \frac{p}{1 - e^{-p}}. \quad \text{(A13)}$$

Therefore, the parameter form of the envelope is given by

$$\frac{y - y_0}{\text{Mod}} = \ln \left(\frac{p}{1 - e^{-p}} \right) + \left(\frac{p}{1 - e^{-p}} \right) - 1 - p\,,$$

$$\frac{x - x_0}{\Delta x} = \frac{1}{p} \left(\frac{p}{1 - e^{-p}} - 1 \right),$$

$$p = \frac{b\Delta x}{\text{Mod}}.$$

Procedure

1. The left-hand side of the sheet film (Fig. A1) contains a number of straight lines that are used to perform the integration

$$\int_{-\infty}^{x_0} f(x)\, dx\,.$$

The sheet film is superposed on the graph so that the point $[x_0; \log f(x_0)]$ lies at the convergent point of these lines. Great care is used to insure that the co-ordinates' axes of the nomograph and of the working graph are parallel. We select the line from this family that best represents $\log f(x_0)$ in the neighborhood of $\log f(x_0)$. The numbers written at the left ends of these lines give the corresponding log (Mod/b) to be added to $\log f(x_0)$ to get

$$\log \int_{-\infty}^{x_0} f(x)\, dx$$

according to equation (A4b). In our example this line corresponds to -0.30. Hence the first point will be

$$\log \int_{-\infty}^{x_0} f(x)\, dx = \log f(x_0) - 0.30 .$$

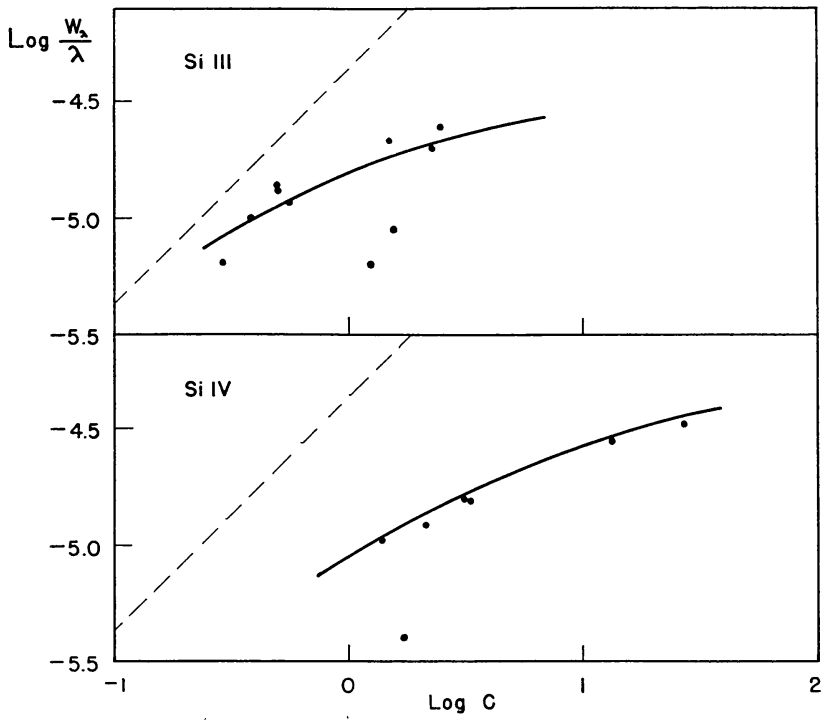

FIG. A1.—Curves of growth for silicon. The lines of Si III and Si IV are among the strongest observed in the spectrum of this star. Some uncertainties are introduced by the collisional damping constants.

This point is entered on the working graph with the co-ordinates $[x_0; \log f(x_0) - 0.30]$. This is the initial point of the log of the integral

$$\int_{-\infty}^{x_0} f(x)\, dx$$

whose curve we will plot.

2. We suppose that beyond x_0 the curve $\log f(x)$ changes its slope so rapidly that we must now integrate step by step. We restrict our discussion to two step-widths, $\Delta x = 0.1$ or 0.2. Let us first treat the problem for $\Delta x = 0.2$.

Just to the right of the vertical line, the family of envelope curves is depicted. Now adjust the sheet film so that the straight-line approximation of $\log f(x)$ in this interval $(x_0 - x_0 + 0.2)$ touches the envelope. With the film held tightly in place, we mark a point through the hole at the $x_0 + 0.2$ position in the film to the right of the value 1.0 in the lower scale. This gives

$$\log \int_{x_0}^{x_0+0.2} f(x)\, dx .$$

3. In order to add

$$\int_{x_0}^{x_0+0.2} f(x)\,dx \qquad \text{to} \qquad \int_{-\infty}^{x_0} f(x)\,dx$$

when we have the functions given in log form, we use the identity

$$\log(A+B) = \log A + \log\left(1+\frac{B}{A}\right),$$

where $A > B$. In our example

$$A = \int_{-\infty}^{x_0} f(x)\,dx \qquad \text{and} \qquad B = \int_{x_0}^{x_0+0.2} f(x)\,dx.$$

To perform this operation, we measure the difference

$$\log A - \log B = D$$

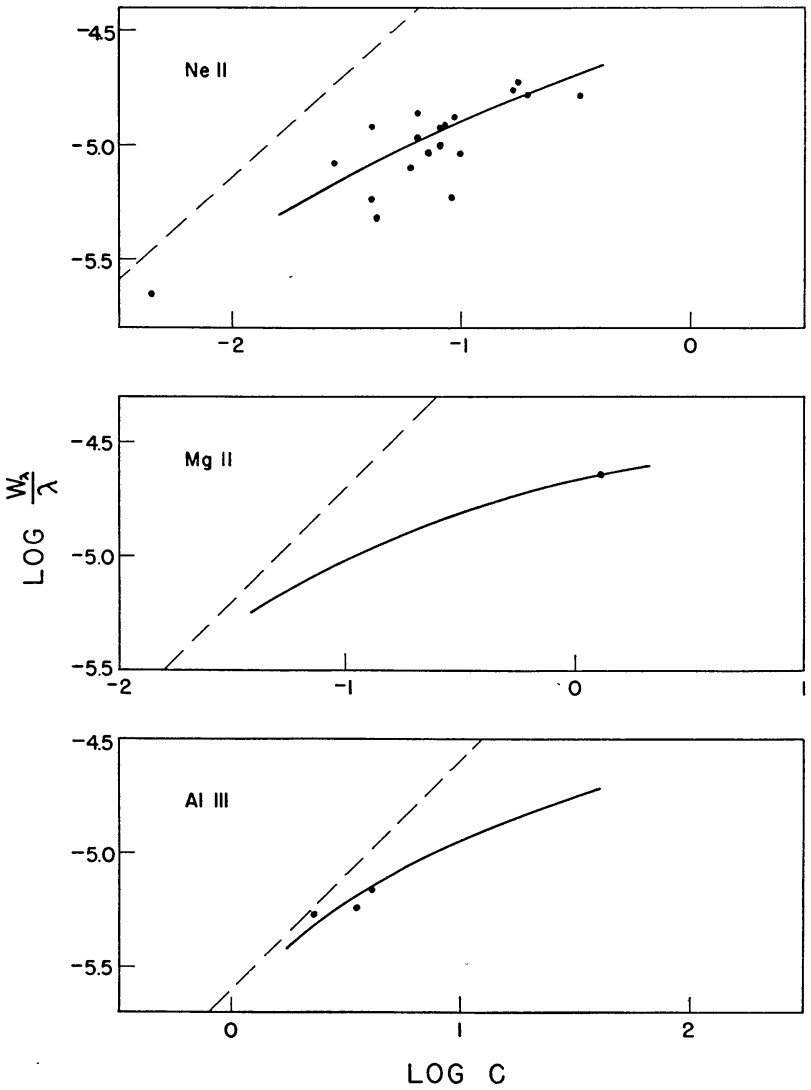

FIG. A2.—Curves of growth for neon, aluminum, and magnesium. These elements are observed in only one stage of ionization as Ne II, Al III, and Mg II.

by adjusting the sheet film as shown in Figure A2. The point log A lies on the horizontal line, 0.2 units (cm) left of the scales; log B falls on the lower scale, where we read $D = 0.25$ in our example. Enter the upper scale with D and mark the point on the graph paper. Since this scale gives log $(1 + B/A)$, the new point on the $(x_0 + 0.2)$ line now gives

$$\log \int_{-\infty}^{x_0+0.2} f(x)\, dx = \log A + \log\left(1 + \frac{B}{A}\right).$$

The next steps of the integration now involve a repetition of steps 2 and 3.

In the case that the step-width $\Delta x = 0.2$ seems too rough, we use the step-width $\Delta x = 0.1$. The only difference in section 2 of this appendix is that tne envelope reduces to the point at the horizontal line indicated by the little arrow and the hole which has to be used lies at the distance $\Delta x = 0.1$ from the lower scale.